



The Ocean-Refraction Bathymetric-Scattering (ORBS) Model

E. B. WRIGHT, D. H. BERMAN, R. N. BAER, AND J. S. PERKINS

*Acoustic Systems Branch
Acoustics Division*

July 29, 1988

REPORT DOCUMENTATION PAGE				Form Approved OMB No. 0704-0188	
1a. REPORT SECURITY CLASSIFICATION UNCLASSIFIED			1b. RESTRICTIVE MARKINGS		
2a. SECURITY CLASSIFICATION AUTHORITY		3. DISTRIBUTION / AVAILABILITY OF REPORT Approved for public release; distribution unlimited.			
2b. DECLASSIFICATION / DOWNGRADING SCHEDULE					
4. PERFORMING ORGANIZATION REPORT NUMBER(S) NRL Report 9123			5. MONITORING ORGANIZATION REPORT NUMBER(S)		
6a. NAME OF PERFORMING ORGANIZATION Naval Research Laboratory		6b. OFFICE SYMBOL (If applicable) Code 5160	7a. NAME OF MONITORING ORGANIZATION		
6c. ADDRESS (City, State, and ZIP Code) Washington, DC 20375-5000			7b. ADDRESS (City, State, and ZIP Code)		
8a. NAME OF FUNDING / SPONSORING ORGANIZATION Office of Naval Research		8b. OFFICE SYMBOL (If applicable)	9. PROCUREMENT INSTRUMENT IDENTIFICATION NUMBER		
8c. ADDRESS (City, State, and ZIP Code) Arlington, VA 22217			10. SOURCE OF FUNDING NUMBERS		
			PROGRAM ELEMENT NO 61153N	PROJECT NO RR011-08-43	TASK NO
			WORK UNIT ACCESSION NO DN 156-016		
11. TITLE (Include Security Classification) The Ocean-Refraction Bathymetric-Scattering (ORBS) Model					
12. PERSONAL AUTHOR(S) Wright, E. B., Berman, D. H., Baer, R. N., and Perkins, J. S.					
13a. TYPE OF REPORT Interim		13b. TIME COVERED FROM Oct 84 TO Sept 87		14. DATE OF REPORT (Year, Month, Day) 1988 July 29	15. PAGE COUNT 43
16. SUPPLEMENTARY NOTATION					
17. COSATI CODES			18. SUBJECT TERMS (Continue on reverse if necessary and identify by block number)		
FIELD	GROUP	SUB-GROUP			
			Acoustic scattering Acoustic model		
			Bathymetric scattering Three-dimensional modeling		
19. ABSTRACT (Continue on reverse if necessary and identify by block number)					
<p>The ocean-refraction bathymetric-scattering (ORBS) model is an underwater acoustic model, implemented on the VAX 11/785 and Cray X-MP/24 computers, that uses two-dimensional spatial frequency spectra of ocean bathymetry to estimate the effect, in the ensemble-average sense, of bottom scattering on the coherence of an acoustic signal. The model is designed for a situation (either long-range or short-range) where one bottom interaction dominates the propagation. The principal output of ORBS is a simulation of the beam response of an acoustic array. The calculation works by propagating an "angular power distribution" (the Fourier transform of the mutual coherence function) along its characteristic curves in the medium. The bottom-interaction calculation is a three-dimensional computation of scattering from a rough bottom described by a two-dimensional power spectral density of bottom heights about a mean slope of arbitrary inclination. To compute the scattering, the model does a modified Kirchhoff calculation from the bottom-roughness spectrum (D. H. Berman and J. S. Perkins, <i>J. Acoust. Soc. Am.</i> 78, 1045-1051 (1985)). An averaged bottom roughness spectrum derived from experimental measurements can be used to predict scattering for particular bottom types.</p> <p style="text-align: right;">(Continues)</p>					
20. DISTRIBUTION / AVAILABILITY OF ABSTRACT <input checked="" type="checkbox"/> UNCLASSIFIED/UNLIMITED <input type="checkbox"/> SAME AS RPT <input type="checkbox"/> DTIC USERS			21. ABSTRACT SECURITY CLASSIFICATION UNCLASSIFIED		
22a. NAME OF RESPONSIBLE INDIVIDUAL Evan B. Wright			22b. TELEPHONE (Include Area Code) (202) 767-3173		22c. OFFICE SYMBOL Code 5160

19. ABSTRACT (Continued)

ORBS uses an approximation to the Kirchoff scattering integral that reduces its computation time by almost two orders of magnitude (D. H. Berman and J. S. Perkins, *J. Acoust. Soc. Am.* **78**, 1024-1028 (1985)). This permits solution of a problem with as many as 10^6 scattering cross-section calculations within a 20-min. run on a VAX-11/785, with the computed scattered power accurate to a fraction of 1 dB (when compared with the results from computing the Kirchoff integral directly).

CONTENTS

PREFACE	v
1. INTRODUCTION	1
2. THE MUTUAL COHERENCE FUNCTION AND ARRAY RESPONSE	2
3. COMPUTING ARRAY RESPONSE WITH BOTTOM-INTERACTING PATHS	5
4. SAMPLE OUTPUTS FROM THE ORBS MODEL	7
5. SUMMARY AND CONCLUSIONS	15
ACKNOWLEDGMENTS	16
REFERENCES	17
APPENDIX A — Coherence Function Definitions and Propagation	19
APPENDIX B — Array Simulation and the Coherence Function	25
APPENDIX C — Tracing the Characteristic Paths	29
APPENDIX D — Computing the Scattering Cross Section	31
APPENDIX E — Program Data Inputs	37

PREFACE

This report presents major developments in a continuing research program in underwater acoustics at the Naval Research Laboratory. These studies, begun in 1974, have investigated the spatial and temporal properties of low-frequency acoustic fields in the ocean. Their objective is to provide a priori estimates of the capabilities of highly directional receiving arrays and the signal coherence as it may be degraded by environmental irregularities. The NRL project initially concentrated on the degradation caused by scattering in the ocean volume. These studies were followed by studies of scattering at its boundaries. Both processes are irreversible and the irregularities causing the scattering are statistically described. The statistical approach is natural for the ocean environment, because the principal parameters exhibit significant departures from their mean values. They vary from place to place in a manner that is statistically stable but difficult to measure in detail. This is true for volume parameters (e.g., sound speed deviations) [1] and for boundary parameters (e.g., bathymetric roughness) [2]. The statistical approach is therefore the appropriate method for predicting the performance of acoustic systems in the ocean. This is especially true for receiver array design tasks such as:

- Predicting an environmentally constrained upper limit on array size to achieve specific performance levels (gain, resolution, and sidelobe suppression).
- Developing a deployment or operational strategy for mobile or fixed arrays. For example, how many systems should be used, where should they be placed, and how are they best oriented, are all questions that this statistical model can help to answer.
- Computing an envelope of array system performance for mobile tactical systems where bottom contact at different attack directions produces an output controlled by the magnitude and orientation of bottom roughness spectra.
- Determining the probability of detecting target echoes or passive radiation with specific system parameters and operating conditions and as a function of the bottom spectral character.

The NRL project has addressed the causes of degradation of spatial coherence of acoustic signals as the key new system issue. This is because substantial investment in technology depends on whether acoustic field properties, driven by tactics, systems, and operating area, will allow the coherent gain that antennas must achieve to be effective. Ocean acoustic volume effects have been dealt with in earlier reports [3-5]. This research should be extended, because scattering mechanisms and higher frequency regimes that were not previously studied are now of significant interest. Although ocean volume scattering is always present in underwater acoustic propagation, it is generally less than bottom scattering at all frequencies. The detailed bottom irregularities affecting an acoustic signal at any given instant usually cannot be known in sufficient detail to correct for the distortion they cause, but it is important to reliably estimate the expected reduction in receiver array performance. This report presents a model whose current version provides estimates of beam spreading of array outputs caused by a single encounter with a hard, rough ocean bottom.

This report describes the theoretical, numerical, and computational basis of a computer model called the ocean-refraction bathymetric-scattering (ORBS) model. This model estimates the effect of

scattering by a rough, stochastically characterized, ocean bottom on the three-dimensional spatial coherence of an acoustic signal. The model allows for a user-defined sound-speed profile in the ocean. This model allows refraction in the water, three-dimensional bathymetric scattering, and specular reflection to be combined realistically in the calculation. This combination gives ORBS a unique computational predictive capability that was previously unavailable. The model displays the computed acoustic field at a specified receiver location in terms of the simulated output of an arbitrarily oriented line array centered there. (With minor modifications, the program could model a more general array type, such as a line array with missing elements or a billboard array.) The computed outputs include the main peak and sidelobe levels of the simulated pattern, the half-power width, and the computed source bearing relative to the array.

In its present form, the model considers cases where one bottom interaction is dominant. With minor modifications, the ORBS model can be adapted to some straightforward variations of this problem, such as single-bounce propagation under rough ocean ice.

THE OCEAN-REFRACTION BATHYMETRIC-SCATTERING (ORBS) MODEL

1. INTRODUCTION

When a sound wave impinges upon a hard rough surface, a significant amount of the incident energy is incoherently scattered. This is an important phenomenon that degrades the performance of acoustic receiving systems operating on a signal field dominated by reflection and scattering from rough bathymetry. An array located over a rough bottom may be insonified by direct refracted arrivals, by reflections from areas on the bottom, and by energy scattered from the bottom. Generally, depending on the acoustic frequency, the source/receiver geometry, and the characteristics of the bottom, any one of these components of the received sound may be dominant. Consequently, if the degradation in array performance caused by bottom scattering, which is usually a very strong diffusing mechanism, is to be evaluated, the contribution of each component must be computed accurately.

The ocean-refraction bathymetric-scattering (ORBS) model computes array response in the acoustic field by propagation of the Fourier-transformed two-point-mutual coherence function of the pressure field (the transform can be thought of as the power distribution in location and direction) along its characteristic trajectories. To compute these refracted trajectories accurately, ORBS allows for a realistic depth-stratified sound-speed profile as input data; a continuous, stratified curvilinear interpolating function then integrates the path elements. The number of paths required is dictated by the number of receiver points on the computed array, the number of beam directions considered, and the need to sample the acoustic field finely enough to integrate the beam power accurately. In a typical problem, tens or hundreds of thousands of characteristics may be required. For each scattered path, a cross section (probability for scattering) must be computed; ORBS uses a modified form of Kirchhoff theory [6] for this. To make the large number of cross-section calculations feasible, the model uses an approximation to the Kirchhoff integral that replaces the numerical integration by a single function evaluation (of the bottom roughness spectrum). This reduces the computation time by almost two orders of magnitude with little loss of accuracy [7].

Because it must deal with scattering out of the plane of the incident wave, the calculation of the characteristics is three-dimensional. To 'start up' this three-dimensional calculation, ORBS ordinarily uses a parabolic equation (PE) model [8] to propagate the sound from the source to the scattering region. In a long-range case, propagation up to the region of the receiver is typically modeled as cylindrically symmetric, and a split-step PE calculation in the range-depth plane is used [9,10]. However, three-dimensional PE models exist [11] and could be used, if appropriate, for this phase of the problem. In a typical short-range, bottom-bounce, active or passive sonar case, the startup field is required at a range of a few kilometers (or less) from the source, and a cylindrically symmetric PE calculation or simulated source field is used.

Section 2 is an overview of the propagation of the coherence function transform in ORBS and its use in computing the directional response of an array. Section 3 describes the model formulation for the redirection of acoustic energy at a scattering point on the bottom. Section 4 presents sample computed results for varying geometries and varying parameters of the two-dimensional spectrum describing the rough bottom. Section 5 is a summary of the report. The important computational algorithms used are described in detail in appendixes, and a guide to program operation is included.

2. THE MUTUAL COHERENCE FUNCTION AND ARRAY RESPONSE

Figure 1 shows the two phases of the ORBS propagation calculation. The first phase comprises the region from the source to the range R_p in the figure. In a short-range bottom-bounce case this region may span only a few kilometers and serve simply to start up the bottom-interaction phase of the calculation. In a long-range, deep-basin case where a sound channel is present, it may span tens or hundreds of miles. The main phase of the calculation is in the region where bottom interaction—in particular, a single bottom bounce—is expected to provide the dominant paths for sound reaching the receiver. Bottom reflections and scattering introduce propagation directions that are not cylindrically symmetric about the source, so a fully three-dimensional calculation is required in this region.

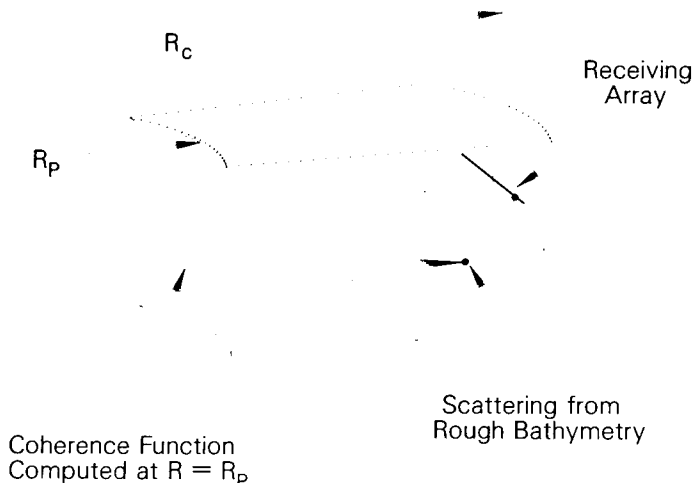


Fig. 1 — The concept of the ORBS propagation algorithm in the bottom interaction region. R_p is the “source cylinder” range, and R_c is the range of the center of the array. A scattered path and a corresponding set of incident paths are shown.

In the first region, before significant bottom interaction is encountered, a two-dimensional model is usually adequate. To start up the ORBS algorithm, the two-dimensional Helmholtz equation for the complex acoustic pressure $p(r, z)$ is approximated in this region by the parabolic equation (PE) [8]

$$2ik_0 p_r + p_{zz} + k_0^2 [n^2(r, z) - 1] p = 0. \quad (1)$$

The coordinate system consists of depth z measured positive downward from the ocean surface and range r measured horizontally from the sound source. In Eq. (1), n is the index of refraction ($n(r, z) = c_0/c(r, z)$, where $c(r, z)$ is the sound speed at the point r, z and c_0 is a reference sound speed), and $k_0 = 2\pi f/c_0$ where f is the source frequency measured in Hz. The parabolic equation is solved by the split-step algorithm [9,10].

Thus, with use of the parabolic equation method, the acoustic field is known at range $r = R_p$ (Fig. 1) as a function of depth. At this range, we form the two-point product of the acoustic field,

$$\Gamma(r, z_1, z_2) = p(r, z_1) p^*(r, z_2),$$

where the asterisk indicates complex conjugation. The two points are at the same range r . The product is now written in mean-and-difference coordinates in depth:

$$z = (z_1 + z_2)/2, \quad s = z_1 - z_2$$

and transformed in the depth-difference coordinate

$$\hat{\Gamma}(r, z, \phi) = \int_{-\infty}^{\infty} \Gamma(r, z + \frac{s}{2}, z - \frac{s}{2}) e^{-isk_0 \sin \phi} ds. \quad (2)$$

$\Gamma(r, z_1, z_2)$ is the two-point mutual coherence function of the complex acoustic pressure field. Its Fourier transform $\hat{\Gamma}(r, z, \phi)$ can be regarded as a power density or distribution in ϕ , with ϕ being the direction of energy propagation in the vertical. This function is useful because there is a transport equation for propagating it, and there is a method of using it to compute array response. In the text that follows, the transformed coherence function is denoted as $\hat{\Gamma}(\mathbf{r}, \hat{\mathbf{k}})$ where \mathbf{r} denotes a point in three-dimensional space and the unit vector $\hat{\mathbf{k}}$ specifies a direction. The relation between $\hat{\Gamma}$ in three dimensions and $\hat{\Gamma}$ defined in a plane is discussed rigorously in Appendix A.

From the Helmholtz or the parabolic equation, a transport equation can be derived for propagating the transformed coherence function. This is a differential equation whose solutions are the characteristic contours, along each of which the value of $\hat{\Gamma}$ is constant. References 5 and 12 provide further discussion of the transformed coherence function and its transport equation.

In the bottom-interaction region, ORBS uses a propagation algorithm based on the fact that the characteristics of the transport equation for $\hat{\Gamma}$ are trajectories computationally identical to the rays of geometric acoustics [12]. Within this limited region, we assume that horizontal variation of the sound speed in the ocean is negligible, i.e., the sound speed is a function of depth only. The angular power distribution at a point on the array is given by the value of $\hat{\Gamma}$ at the point. This is computed by tracing a discrete set of characteristics (rays) from points along the array backward to the "source cylinder" where the characteristic value of $\hat{\Gamma}$ for each path can be evaluated. This source cylinder is defined by $r = R_p$. To compute the total field, it is necessary to include contributions from paths specularly reflected from the bottom, from paths scattered by it, and from direct waterborne paths (those not encountering the bottom). The backward-looking algorithm is used for computational efficiency; it guarantees that the program never needlessly computes paths that do not reach the array.

The program thus computes $\hat{\Gamma}$ at a set of discrete points, which can be regarded as hydrophones in an array. (We consider a linear array here for simplicity and because it represents the current implementation of the model.) The next step is to compute the magnitude of the directional array response, usually defined as

$$A(\theta) = \int_{-L/2}^{L/2} w(Y) p(Y) \exp(-ik_0 Y \sin \theta) dY, \quad (3)$$

where Y is the coordinate locating a point on the array, $p(Y)$ is the acoustic pressure, k_0 is the acoustic wave number, θ is the steering angle, L is the array length, and $w(Y)$ is the weighting function used in the beamforming. Appendix B shows that the angular power distribution observed by the array can be written as a weighted integral of $\hat{\Gamma}$ over the array:

$$\langle |A(\theta)|^2 \rangle = \int \int \int a(Y, \psi, \theta) \hat{\Gamma}(\mathbf{Y}, \hat{\mathbf{k}}) \cos \psi \, d\psi \, d\Omega \, dY, \quad (4)$$

where $a(Y, \psi, \theta)$ is computed from $w(Y)$. This observed intensity distribution is an ensemble average arising from the stochastic description of the rough bottom. The angles ψ and Ω specify the direction of $\hat{\mathbf{k}}$ in a coordinate system to be defined next.

The array may be yawed and/or tilted with respect to the fixed coordinate system in the ocean. It is convenient to define directions of paths traced from a point on the array in a coordinate system that is fixed with respect to the array. Figure 2 shows the unit vector $\hat{\mathbf{k}}'$, the initial direction of a path traced from point P on the array. (The unit vector $\hat{\mathbf{k}} = -\hat{\mathbf{k}}'$ is the local direction of the wave vector on this path.) In Fig. 2, ψ is measured from a plane whose normal is the array axis; it is a beam angle measured from broadside. All unit vectors $\hat{\mathbf{k}}'$ having a common beam angle ψ describe a right circular cone, and Ω is the angle defining the direction within the cone. These coordinates are chosen because a linear array cannot distinguish among different arrivals having a common beam angle. ORBS samples the acoustic field by tracing out a two-dimensional array of paths at equal increments in ψ and Ω . Each path is traced to its intersection with the bottom (paths not interacting with the bottom are a special case to be discussed below). Appendix C describes the tracing formulas used in the model.

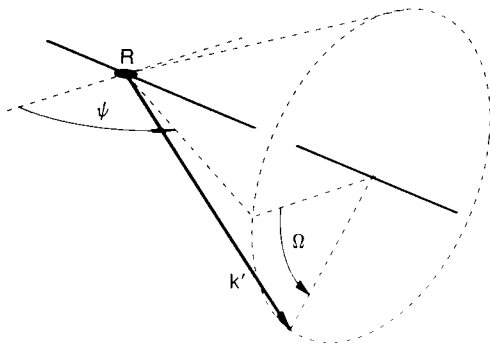


Fig. 2 — Angular coordinates defining a path direction with respect to the array. All unit vectors k' at point R on the array, with beam angle ψ , form a cone. Contributions from all angles Ω within the cone are summed.

Because ORBS uses a receiver-to-source propagation algorithm, it expresses the power propagated by each scattered path as a weighted summation over all possible paths from the source to the scattering point. The weighting function in this summation is the differential cross section for scattering from the rough bottom and is discussed in Section 3. The program also tests for the existence of a specular reflection at each bottom scattering point and computes the appropriate reflection coefficient whenever a reflected path is found.

The special case of paths not interacting with the bottom is simpler because each path can be traced directly back to the source cylinder in a single vertical plane. (This follows from the assumption that the sound speed depends only on depth in the bottom-bounce region.) The refracted-only part of the calculation accounts for a small part of the computer time, most of which goes to computing the large set of incident paths for each scattered path.

The essential features of the ORBS propagation algorithm can be summarized as:

- A wave model is used to propagate the acoustic field from the source to the bottom-bounce region. At this point, the mutual coherence function and its Fourier transform $\hat{\Gamma}$ are computed, because a raylike transport equation for $\hat{\Gamma}$ exists and because $\hat{\Gamma}$ can be used to compute array response.
- Ray computations are used to propagate the field through this bottom-bounce region, so that a fully three-dimensional calculation of the refracted, coherently reflected, and incoherently scattered paths can be made there. Also, the array and the mean bottom plane may both be oriented arbitrarily. In principle, any array configuration could be represented by a straightforward modification of the program.
- The raylike computation of bottom-scattered paths permits the use of Kirchhoff theory to compute the scattering cross section as a weight for each path when the paths are summed at the array. Thus the resulting summation includes a stochastic ensemble average of the angular power distribution of bottom-scattered energy received at the array. This distribution function is used to compute a simulated array response.

3. COMPUTING ARRAY RESPONSE WITH BOTTOM-INTERACTING PATHS

This section shows how the array response integral of Eq. (4) is formulated when the function $\hat{\Gamma}$ in the integrand is computed from paths that are bottom-reflected or scattered between the source and the array. These calculations require transformations between different coordinate systems and transformations of the arguments of delta functions in the integrands, which may introduce nontrivial Jacobian factors.

Figure 3 shows the geometry of the problem. We assume that a single sound speed profile characterizes the bottom-interaction region, so that each path traced (at least until it contacts a boundary) is confined to one vertical plane. This plane, labeled P_R , contains a point R on the array and a scattering point B in the mean bottom plane. (The angle α is the yaw of the array.) The vertical plane P_S contains B and the source S . The angles θ and δ specify the azimuths of the two planes, and $\hat{\mathbf{n}}_R$ and $\hat{\mathbf{n}}_S$ are the respective unit normals. Thus the figure defines the propagation planes for two traces, P_S for an incident path and P_R for a scattered (or reflected) path. The two paths meet at point B , as shown in Fig. 4. Unit vectors $\hat{\mathbf{q}}$ and $\hat{\mathbf{k}}$ are the directions of the incident and scattered paths, respectively, at B .

It is convenient to define the directions of $\hat{\mathbf{q}}$ and $\hat{\mathbf{k}}$ in a coordinate system that is fixed with respect to the bottom at B , because the scattering cross section is a function of the incident and scattered angles in such a system. Figure 4 shows the system we use; its basis is the set of unit vectors $[\hat{\mathbf{n}}, \hat{\mathbf{p}}, \hat{\mathbf{d}}]$, where $\hat{\mathbf{n}}$ is the normal to the mean bottom plane, $\hat{\mathbf{p}}$ is the downslope direction in the mean bottom plane, and $\hat{\mathbf{d}} = \hat{\mathbf{n}} \times \hat{\mathbf{p}}$ (making $\hat{\mathbf{d}}$ horizontal). The incoherent part of $\hat{\Gamma}$ in the scattered direction can be expressed as an integral over incident directions, where θ_q is the polar angle measured from $\hat{\mathbf{d}}$ and ϕ_q is an azimuth measured from $\hat{\mathbf{p}}$:

$$\hat{\Gamma}_{\text{scat}}(\mathbf{r}_B, \hat{\mathbf{k}}) = \int_0^\pi \sin \theta_q \int_{-\frac{\pi}{2}}^{\frac{\pi}{2}} \frac{\sigma(\mathbf{q} \rightarrow \mathbf{k})}{\hat{\mathbf{n}} \cdot \hat{\mathbf{k}}} \delta(\hat{\mathbf{q}} \cdot \hat{\mathbf{n}}_s) \hat{\Gamma}(\mathbf{r}_B, \hat{\mathbf{q}}) d\phi_q d\theta_q, \quad (5)$$

where \mathbf{r}_B is the location of the scattering point, $\sigma(\mathbf{q} \rightarrow \mathbf{k})$ is the differential cross section per unit area for scattering from \mathbf{q} into \mathbf{k} (see Appendix D), and the delta function requires that each incident

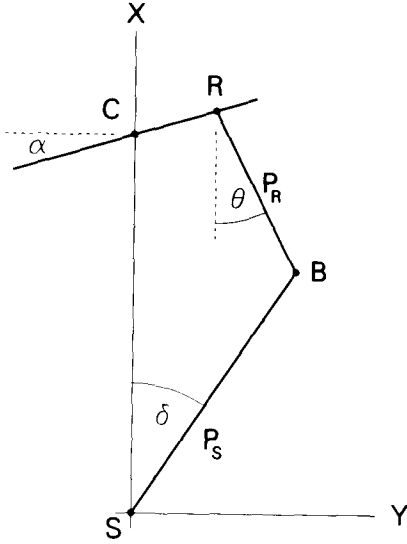
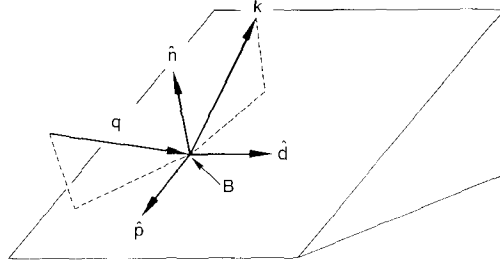


Fig. 3 — The coordinate system used in the propagation calculation. The z -axis is positive downward (into the page). The angles δ and θ are azimuths of the vertical planes of the antecedent and scattered paths, respectively. The angle α is the yaw of the array (rotation about a vertical axis, from broadside).

Fig. 4 — The antecedent and scattered directions at the bottom point B are defined by wave vectors \mathbf{q} and \mathbf{k} , respectively. The bottom-fixed coordinate system $[\hat{\mathbf{n}}, \hat{\mathbf{p}}, \hat{\mathbf{d}}]$ is shown.



vector \mathbf{q} must lie in P_S . The integral of Eq. (5) can be evaluated by some manipulations that simplify the delta function so that the integration over ϕ_q can be performed. The resulting integral over θ_q is easily transformed to an integral over ϕ , the vertical angle of the incident direction in P_S :

$$\hat{\Gamma}_{\text{scat}}(\mathbf{r}_B, \hat{\mathbf{k}}) = \int_{-\pi/2}^{\pi/2} \frac{\sigma(\mathbf{q} - \mathbf{k})}{\hat{\mathbf{n}} \cdot \hat{\mathbf{k}}} \hat{\Gamma}(\mathbf{r}_B, \hat{\mathbf{q}}(\phi)) d\phi. \quad (6)$$

From Eq. (4) the array response as a function of steering angle θ caused by the incoherent part of the acoustic field is written

$$\langle |A(\theta)|^2 \rangle_{\text{scat}} = \iiint a(Y, \psi, \theta) \hat{\Gamma}_{\text{scat}}(\mathbf{r}_B(Y, \psi, \Omega), \hat{\mathbf{k}}(Y, \psi, \Omega)) \cos \psi d\psi d\Omega dy \quad (7)$$

where $\hat{\Gamma}_{\text{scat}}(\mathbf{r}_B, \hat{\mathbf{k}})$ is given by Eq. (6). Equation (7) explicitly shows the dependence of \mathbf{r}_B , $\hat{\mathbf{q}}$, and $\hat{\mathbf{k}}$ on Y , ψ , and Ω (the location and direction of the scattered path at the array).

Now consider the contribution of the specularly reflected part of the field, which can be written (from Eq. (4))

$$\langle |A(\theta)|^2 \rangle_{\text{refl}} = \iiint a(Y, \psi, \theta) \hat{\Gamma}(\mathbf{r}_B(Y, \psi, \Omega), \hat{\mathbf{k}}(Y, \psi, \Omega)) \cos \psi d\psi d\Omega dY. \quad (8)$$

When $\hat{\Gamma}(\mathbf{r}_B, \hat{\mathbf{k}})$, the characteristic value on the reflected path, is computed by evaluating the value on the incident path, Eq. (8) becomes

$$\langle |A(\theta)|^2 \rangle_{\text{refl}} = \int \int \int a(Y, \psi, \theta) \hat{\Gamma}(\mathbf{r}_B(Y, \psi, \Omega), \hat{\mathbf{k}}(Y, \psi, \Omega)) \delta(\hat{\mathbf{q}}_{\text{refl}} - \hat{\mathbf{n}}_s) \cos \psi d\psi d\Omega dY, \quad (9)$$

where $\hat{\mathbf{q}}_{\text{refl}}$ must be in the specular direction:

$$\hat{\mathbf{q}}_{\text{refl}}(Y, \psi, \Omega) = \hat{\mathbf{k}}(Y, \psi, \Omega) - 2\hat{\mathbf{n}}[\hat{\mathbf{n}} \cdot \hat{\mathbf{k}}(Y, \psi, \Omega)].$$

Again, the notation indicates that the location \mathbf{r}_B and the directions $\hat{\mathbf{k}}$ and $\hat{\mathbf{q}}$ of the reflected and incident paths at B are functions of the location and direction of the reflected path at the array. The delta function requires that the incident path producing the reflection be in the vertical plane containing the source; otherwise the integral must vanish. As above, some manipulation of the delta function is used to facilitate the integration over one variable in the multiple integral. The result is an integral over Ω and Y :

$$\langle |A(\theta)|^2 \rangle = \sum_i \int \int a(Y, \psi_i(\Omega), \theta) \frac{\hat{\Gamma}(\mathbf{r}_B(Y, \psi_i(\Omega), \Omega), \hat{\mathbf{q}}(Y, \psi_i(\Omega), \Omega))}{\left| \frac{2}{2\psi} \hat{\mathbf{n}}_s \cdot \hat{\mathbf{q}}_{\text{refl}}(Y, \psi, \Omega) \right|_{\psi = \psi_i(\Omega)}} \cos \psi_i d\Omega dY. \quad (10)$$

Here, the derivative in the denominator can be approximated numerically by tracing a path having a slightly different value of ψ whenever a specular reflection is found. Ordinarily only one solution $\psi_i(\Omega)$ exists.

4. SAMPLE OUTPUTS FROM THE ORBS MODEL

In this section we present the results of some sample ORBS calculations. The first case uses environmental data from the vicinity of the Gorda Rise in the northeastern Pacific (near 43°N, 127°W), an area whose bathymetry has been extensively mapped and statistically analyzed [2,13]. Roughness ‘‘provinces’’ in the region have been found with spatial amplitude spectra having a power-law dependence, in the formulation of Ref. 2,

$$A(k) \sim k^{-b},$$

where k is the spatial wave number and $1 < b < 2$. An amplitude spectrum in Ref. 2 with a power law coefficient $b = -1.5$ corresponds to a roughness spectral density function in our formulation (see Appendix D)

$$S(k) \sim k^{-4}.$$

Accordingly, we model the ocean bottom in a typical subarea of the Gorda Rise with the roughness spectrum and correlation function (its two-dimensional Fourier transform)

$$S(k) = 4\pi(\sigma L)^2/[1 + (kL)^2]^2,$$

and

$$W(r) = (r/L) K_1(r/L),$$

where σ is the rms residual bottom height and L is a correlation length. L may be taken to correspond to the longest spatial wave length observed in the subarea (i.e., its size) and σ is the total rms residual height over all k -space. K_1 is the modified Bessel function of the second kind.

Figure 5 shows the geometry used for the sample calculations. The mean ocean bottom is a horizontal plane of depth 2972 m. A 1 kHz beamed source S is at a depth of 100 m. The receiving array is at C , also at a depth of 100 m. The source beam pattern is aimed 15° down, with a half-power width of 5° . Figure 6 is a gray-scale plot showing the result of a parabolic-equation intensity calculation for this problem, with a highly reflective bottom (20° critical angle). The shading in each range-depth cell denotes the intensity relative to cylindrical spreading; darker shading means higher intensity. Figure 7 is a similar plot. However, for the PE calculation, bottom roughness here is introduced by pseudorandom variation of the interface depth about the mean bottom depth, with an rms residual roughness of 20 m and a correlation length of 400 m. The rough bottom thus generated is one realization of an ensemble of bottoms characterized by these statistical parameters. (The ORBS calculations to follow are, of course, based upon the statistics of ensemble averages.) Although the two figures have the same general features, Fig. 7 clearly shows bottom scattering and qualitatively suggests deterioration of coherence in the reflected and scattered field.

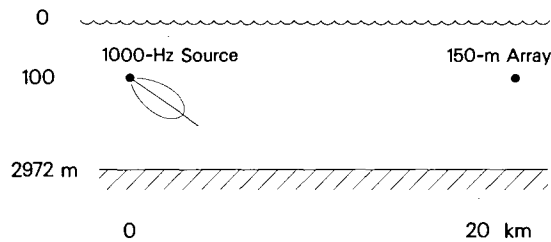


Fig. 5 — Configuration for the sample calculations of Figs. 6 to 16. A beamed 1 kHz source is at S , and the receiving array, which may be horizontal or vertical, is centered at C .

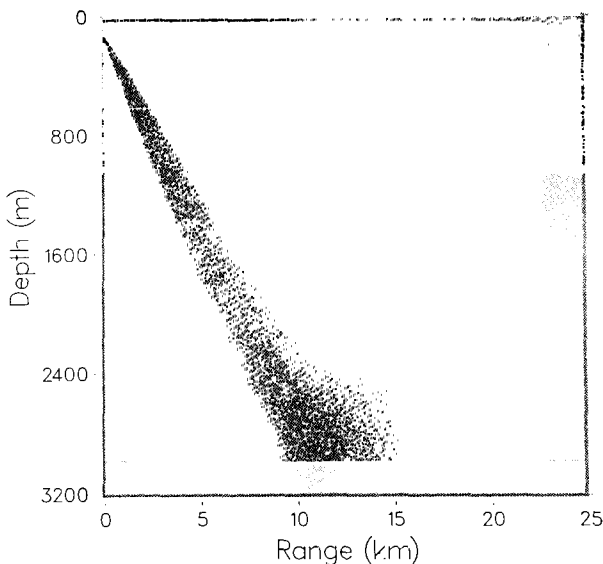


Fig. 6 — Gray-scale intensity plot for the sample problem, from a parabolic equation calculation with the Gorda Rise environment and a smooth reflective bottom

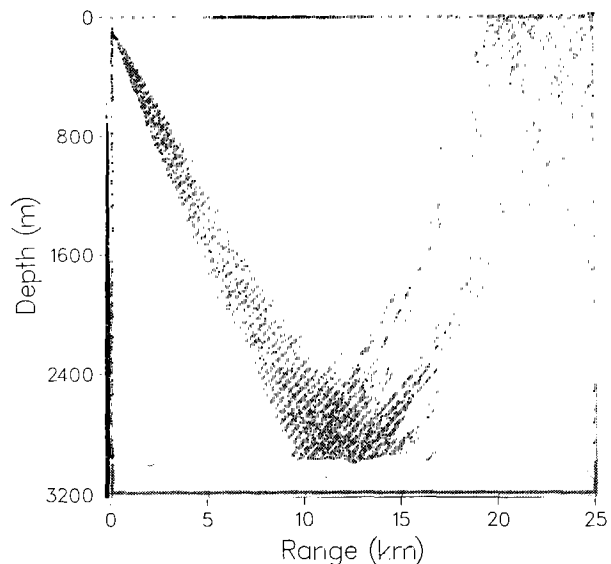


Fig. 7 — Gray-scale intensity plot, similar to Fig. 6, with the smooth bottom replaced by a deterministic rough bottom

The receiver in the problem is a 150-m array centered at a depth of 100 m and oriented either vertically or horizontally. In Figs. 8 and 9 the array is at a range of 20 km, in the beam of bottom-reflected energy, and horizontal. In Fig. 8 ORBS has averaged, over the 21 phones in the array, the relative beam levels for the smooth-bottom case of Fig. 6, i.e., the received energy reaches the array by coherent reflection. Figure 9 is an analogous plot for a rough-bottom case with the parameters of Fig. 7, i.e., the received energy reaches the array by bottom-scattered paths. (The power levels on these plots are relative to the same arbitrarily normalized source level.) The peak of Fig. 9 is ~ 8 dB lower and 2° broader than the peak of Fig. 8. Figure 10 shows the array-processed beam patterns corresponding to the two cases superimposed on a single graph. (Appendix B describes our algorithm for array simulation.) The half-power width increases from 0.4° for the reflected case to 2.5° for the scattered case.

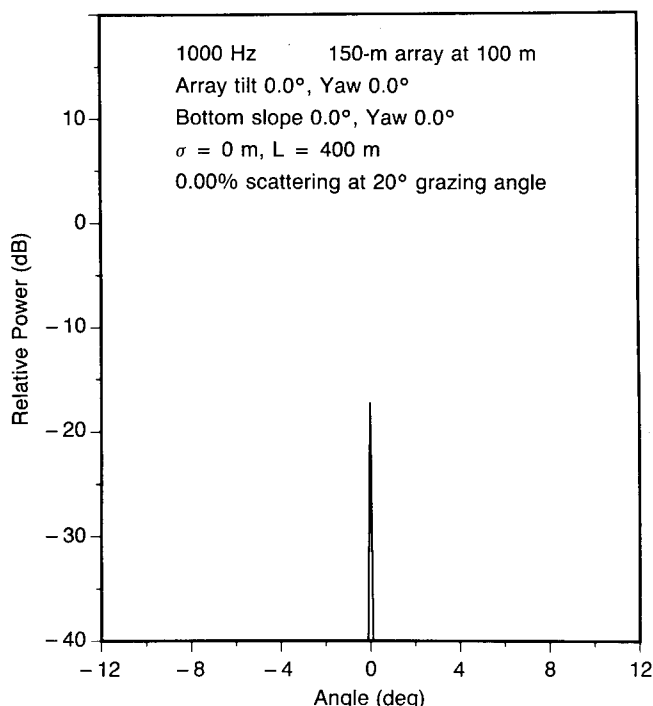


Fig. 8 — Directional distribution of received energy with horizontal receiving array at 20-km range and smooth reflective bottom

In Figs. 11 and 12, the array is vertical and the mean phone levels are computed (as in Figs. 6 and 7). Figure 11 is the smooth-bottom case at 20 km,* and Fig. 12 is the rough-bottom case. Once again, the peak is lowered and broadened in the rough-bottom case. Figures 13 and 14 show the horizontal array at a range of 15 km, at the edge of the zone between the source and the first strong bottom-reflected returns. Not surprisingly, the received level in the reflected case (Fig. 13) is 8 dB lower than at 20 km. However, in the scattered case (Fig. 14), the peak level has dropped only 3.6 dB, showing that a rough bottom scatters a significant amount of energy into the otherwise unsonified region. In fact, at shorter ranges in this region, scattered energy is received where the reflected energy has virtually disappeared. Figure 15 summarizes this effect by plotting the relative maximum beam levels at the horizontal array as functions of range for the reflected and scattered cases. The reflected energy disappears for ranges < 14 km, while in the scattered case energy still appears here.

*The sharp cutoff at 17° in Fig. 11 results from the cutoff in the eigenray set in the smooth-bottom case.

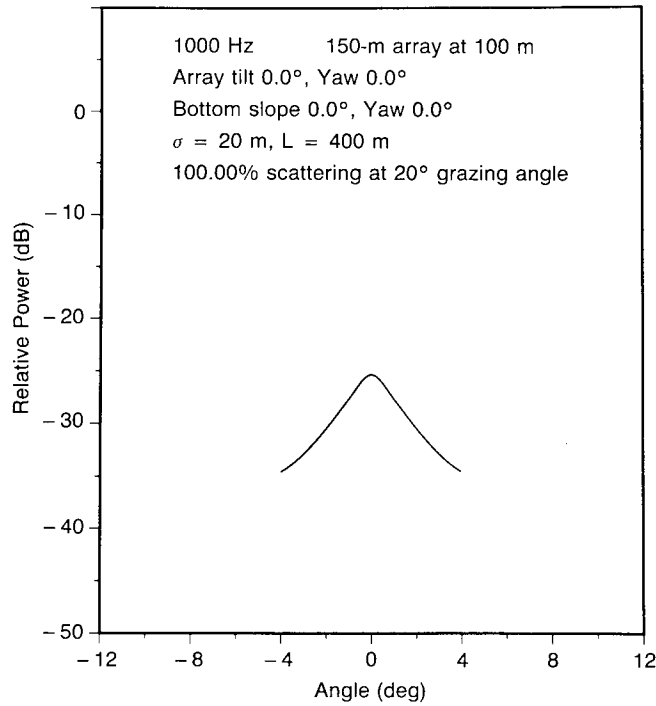


Fig. 9 — Directional distribution of received energy for the sample problem with the horizontal receiving array at 20 km range and stochastic bottom scattering. The source level is the same as in Fig. 8.

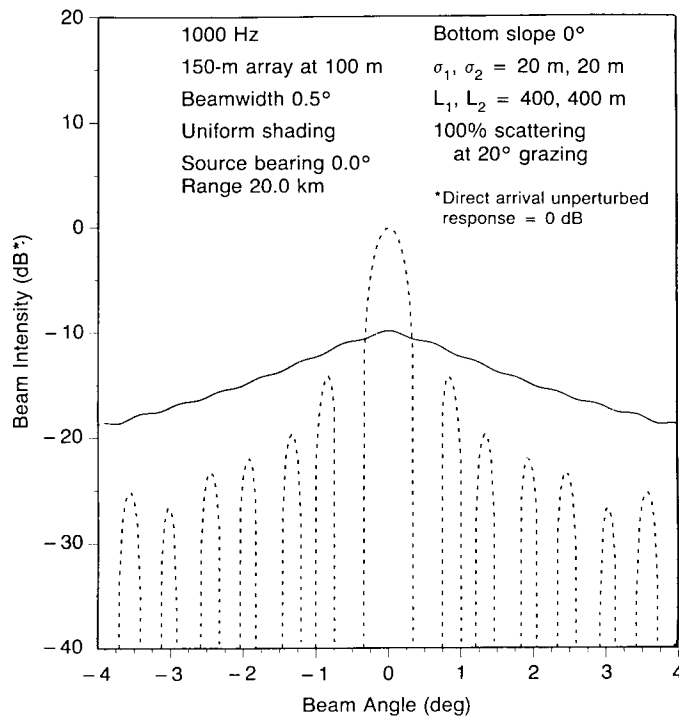


Fig. 10 — Array-simulated beam response patterns corresponding to Figs. 8 and 9. The dashed curve is for the smooth bottom ($\sigma = 0$) and the solid curve is for the rough bottom ($\sigma = 20$ m).

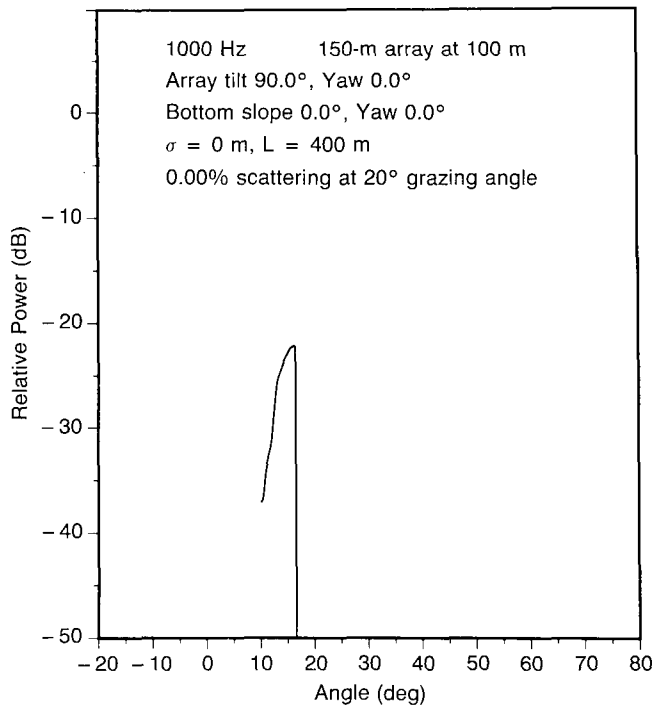


Fig. 11 — Directional distribution of received energy for the sample problem with vertical receiving array at 20 km range and smooth reflective bottom. The source level is the same as in Fig. 8.

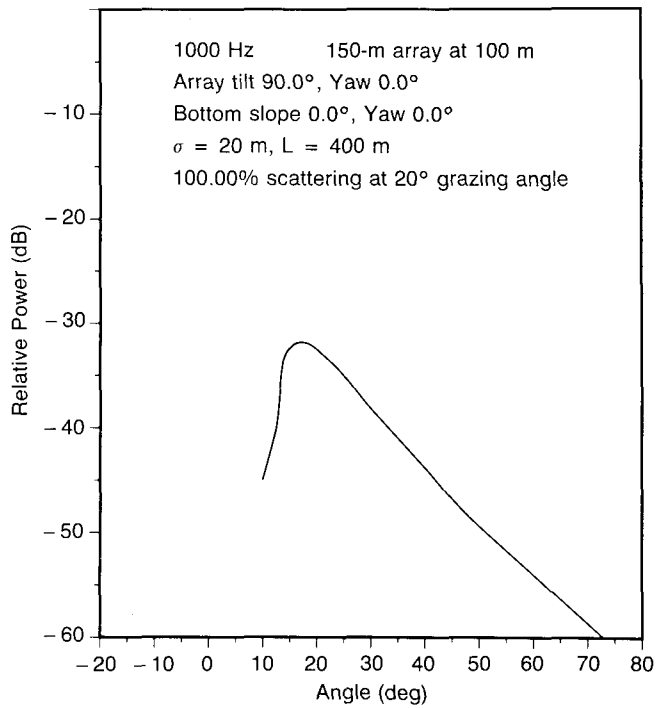


Fig. 12 — Directional distribution of received energy for the sample problem with vertical receiving array at 20 km range and stochastic bottom scattering. The source level is the same as in Fig. 8.

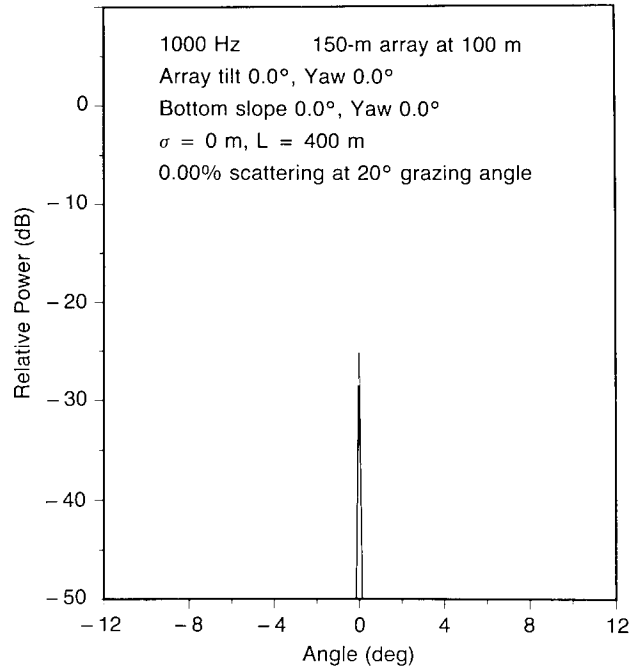


Fig. 13 — Directional distribution of received energy for the sample problem with vertical receiving array at 15 km range and smooth reflective bottom. The source level is the same as in Fig. 8.

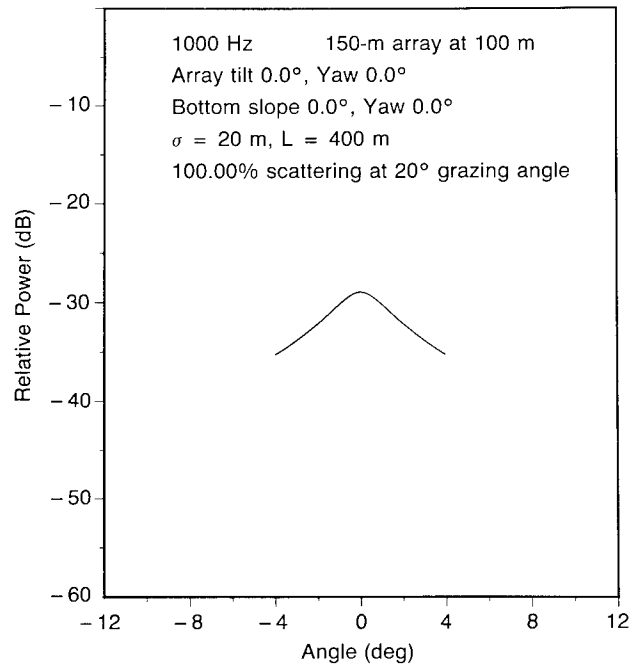


Fig. 14 — Directional distribution of received energy for the sample problem with vertical receiving array at 15 km range and stochastic bottom scattering. The source level is the same as in Fig. 8.

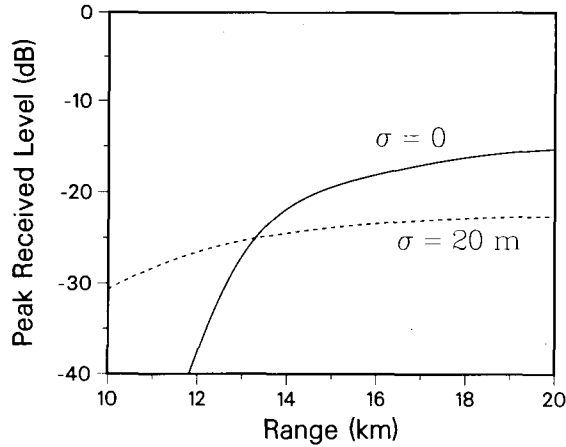


Fig. 15 — Level of peak arrival at horizontal array as a function of range for a smooth bottom ($\sigma = 0$) and a stochastic scattering bottom ($\sigma = 20$ m) in the shadow-zone region for the Gorda Rise case

Figure 16 shows the geometry for a second set of calculations. A 100 Hz source is at a depth of 100 m, 216 km from a 360-m horizontal array at a depth of 2700 m. The bottom slopes downward, away from the array, at an angle of 15° . The bottom is characterized by the same isotropic correlation function used in the short-range problem, but both σ and L are allowed to vary. Figure 17 shows a family of plots of array signal gain (ASG) vs rms roughness, with the bottom correlation length as a parameter. Figure 18 is an analogous plot of half-power width. In both figures, σ and L are expressed in units of the acoustic wavelength, and direct arrivals are omitted. Because the scattering cross-section formulas contain only the ratios of these parameters to the wavelength, the calculations are independent of frequency. They encompass a wide range of values for σ and L . For a 24-wavelength horizontal array in this configuration, the curves predict good performance (ASG within ~ 2 dB of reference level) when $\sigma/\lambda < 2$ and $L/\lambda > 120$. At 100 Hz, these values are about the same as those used in the Gorda Rise example.

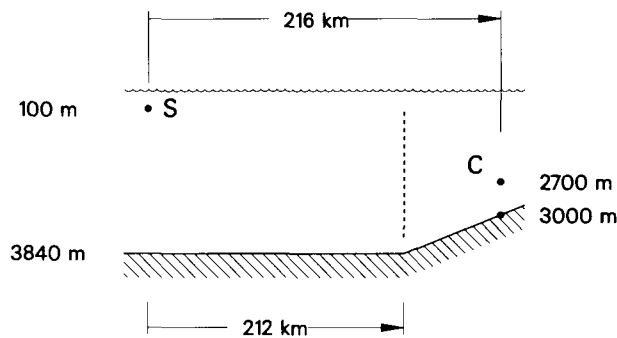


Fig. 16 — Source-receiver configuration for the calculations of Figs. 18 to 21. The source is at S ; the horizontal array is centered at C .

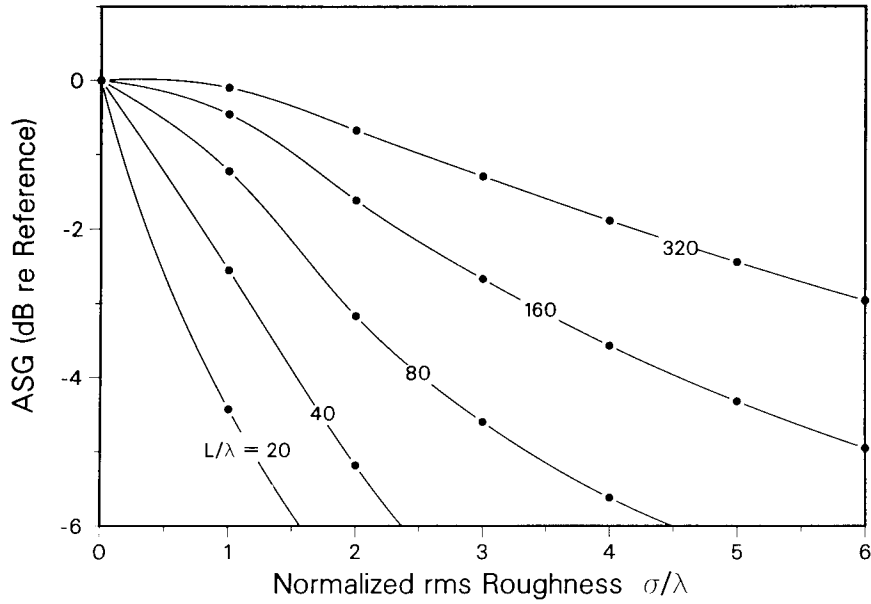


Fig. 17 — Array signal gain as a function of rms bottom roughness for several values of isotropic bottom-height correlation length. Lengths are normalized by wavelength; only the scattered energy is included in the computation.

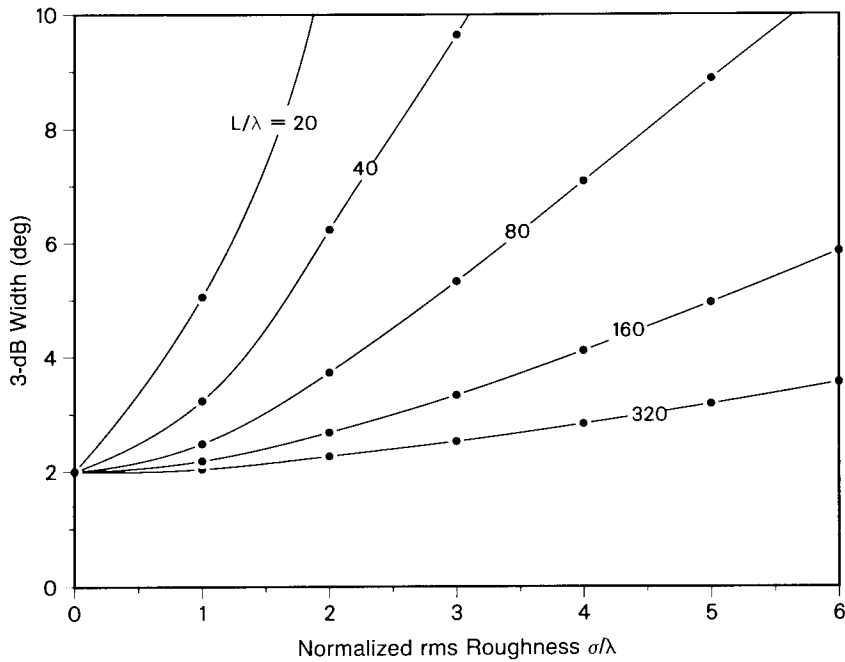


Fig. 18 — Half-power beamwidth as a function of rms bottom roughness for several values of isotropic bottom-height correlation length. Lengths are normalized by wavelength; only the scattered energy is included in the computation.

Finally, Figs. 19 and 20 illustrate cases where the bottom height spectrum is anisotropic, i.e., the correlation lengths L_x and L_y in the mean bottom plane are different (see Appendix D). In this context the x -direction is upslope in the bottom plane, and the y -direction is transverse to the slope. Again, direct arrivals are omitted. The plots show that the scattering is strongly dependent on the transverse correlation length and virtually independent of the slopewise correlation length. Since neither bottom nor array is yawed in these calculations, the upslope direction is perpendicular to the array. The results show that although scattering in the vertical may change the level of sound radiation reaching a horizontal array, it does not affect the detected directionality.

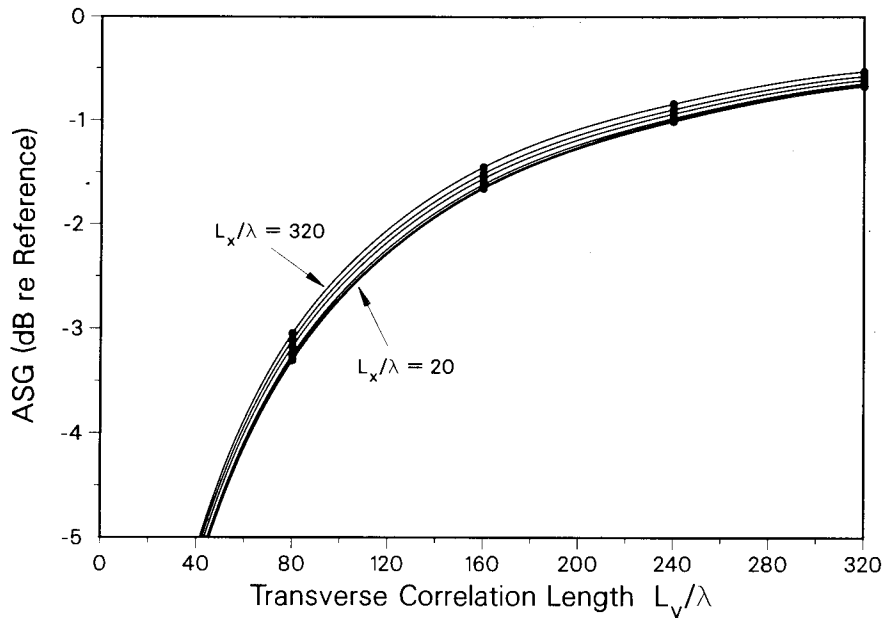


Fig. 19 — Array signal gain for an anisotropic rough bottom. L_x and L_y are the bottom-height correlation lengths, parallel and perpendicular, respectively, to the propagation direction. Lengths are normalized by wavelength; only the scattered energy is included in the computation.

5. SUMMARY AND CONCLUSIONS

We have described a practical model that predicts statistically the effect of rough-bottom acoustic scattering in situations where one bottom interaction is dominant. The ORBS model permits the use of measured environmental data for the sound-speed structure and bottom-roughness statistics, so that realistic calculations can be made for specific ocean areas. The bottom is characterized in the model by a basic and widely used measure of roughness, the power spectral density of residual bottom-height variations in the spatial frequency domain. This roughness spectrum requires only a few parameters, and its functional form in the program can readily be changed to conform to experimentally measured spectra. Refraction in the water column, bottom reflection and scattering in three dimensions, and (optionally) anisotropic bottom roughness are all considered in the model.

The report also demonstrates the application of an exponential substitution method that provides an accurate and computationally efficient approximation for the Kirchhoff scattering integral for large values of rms roughness. The approximation takes about 1% of the time required for numerical evaluation of the integral. With this approximation, a problem involving a total of about 10^{-6} scattering paths requires about 30 min of CPU time on the VAX-11/780 computer. (The present code does not use an array processor.)

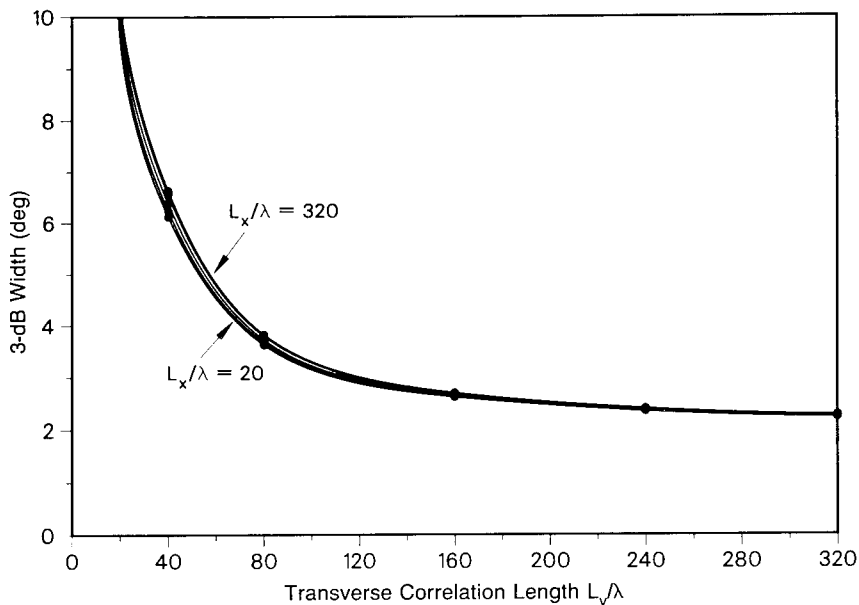


Fig. 20 — Half-power beamwidth for an anisotropic rough bottom. L_x and L_y are the bottom-height correlation lengths, parallel and perpendicular, respectively, to the propagation direction. Lengths are normalized by wavelength; only the scattered energy is included in the computation.

The short-range sample calculation in Section 4 shows the use of the model in a realistic Pacific Ocean environment with known bottom roughness characteristics. ORBS computed the ensemble-averaged directional distribution of energy that is forward-scattered into the region between the source and the first strong bottom reflections. For a smooth reflecting bottom, very little energy reaches this region. When incoherent scattering is included in the calculation, the peak angular level at the receiver has dropped only ~ 8 dB at a point 4 km within the region. The ability to make this stochastic calculation in three dimensions makes ORBS a unique predictive model. Average directional distributions can be calculated with deterministic models by Monte Carlo methods, but this requires considerably more computer effort, especially if done three-dimensionally.

The second sample case shows how the model can be used for practical array design. For a particular configuration of source, ocean bottom, and receiver, the results of several ORBS runs are used to produce graphs relating array performance to the roughness parameters. For example, for a 360-m array at 100 Hz, array signal gain is within 2 dB of reference level when the rms bottom roughness $\sigma < 30$ m and the correlation length $L > 2000$ m. Several other combinations of array and bottom roughness parameters can be used for such studies to evaluate the effect of ocean bottom roughness on array performance.

The methods used in this three-dimensional boundary-scattering model can be applied to other, more general, problems. One multiple-bounce situation is underice sound propagation in the Arctic where the rough boundary is at the surface and the bottom is not encountered; the coherence function approach can be applied here also.

ACKNOWLEDGMENTS

We thank Budd B. Adams and Edward R. Franchi for helpful comments on the text of this report, and for their general guidance and support. We also thank Susan Byron for running the test cases in Section 4. This work was supported by the Naval Research Laboratory, an activity of the Office of Naval Research.

REFERENCES

1. Stanley M. Flatté, ed., *Sound Transmission through a Fluctuating Ocean* (Cambridge University Press, 1979).
2. C.G. Fox and D.E. Hayes, "Quantitative Methods for Analyzing the Roughness of the Seafloor," *Rev. Geophys.* **23**, 1-48 (1985).
3. L.B. Palmer, D.M. Dundore, B.B. Adams, and J.J. McCoy, "Transverse Horizontal Coherence and Low-Frequency Array Gain Limits in the Deep Ocean," NRL Report 8695, Aug. 1983.
4. J.S. Perkins, B.B. Adams, and J.J. McCoy, "Vertical Coherence Along a Macroray Path in an Inhomogeneous Anisotropic Ocean," NRL Report 8792, Aug. 1984.
5. R.N. Baer, J.S. Perkins, E.B. Wright, and J.J. McCoy, "Stochastic Propagation of the Mutual Coherence Function in the Deep Ocean," *J. Acoust. Soc. Am.* **75**, 1407-1414 (1984).
6. D.H. Berman and J.S. Perkins, "The Kirchhoff Approximation and First-Order Perturbation Theory for Rough-Surface Scattering," *J. Acoust. Soc. Am.* **78**, 1045-1051 (1985).
7. D.H. Berman and J.S. Perkins, "Exponential Substitution for Kirchhoff Scattering from Gaussian Rough Surfaces," *J. Acoust. Soc. Am.* **78**, 1024-1028 (1985).
8. F.D. Tappert, "The Parabolic Approximation Method," in *Wave Propagation and Underwater Acoustics*, J.B. Keller and J.S. Papadakis, eds., Lecture Notes in Physics, Vol. 70, pp. 224-286, (Springer-Verlag, New York, 1977).
9. F. Tappert and R. Hardin, in "A Synopsis of the AESD Workshop on Acoustic-Propagation Modeling by Non-Ray-Tracing Techniques, 22-25 May 1973, Washington, D.C.," C.W. Spoford, ed., Acoustic Environmental Support Detachment, Office of Naval Research, Technical Note TN-73-05, pp. 14-16 (Nov. 1973).
10. J.S. Perkins, R.N. Baer, E.B. Wright, and L.F. Roche, "Solving the Parabolic Equation for Underwater Acoustic Propagation by the Split-Step Algorithm," NRL Report 8607, Aug. 1982.
11. J.S. Perkins and R.N. Baer, "An Approximation to the Three-Dimensional Parabolic-Equation Method for Acoustic Propagation," *J. Acoust. Soc. Am.* **72**, 515-522 (1982).
12. J.J. McCoy and M.J. Beran, "Directional Spectral Spreading in Randomly Inhomogeneous Media," *J. Acoust. Soc. Am.* **66**, 1468-1481 (1979).
13. T.E. Chase, P. Wilde, W.R. Normark, C.P. Miller, D.A. Seckins, and J.D. Young, "Offshore Topography of the Western United States between 32° and 49° North Latitudes," Plate 2, U.S. Geol. Survey Open File Map, 81-443 (1981).
14. M.A. Pedersen and D.F. Gordon, "Normal-Mode Theory Applied to Short-Range Propagation in an Underwater Acoustic Surface Duct," *J. Acoust. Soc. Am.* **37**, 105-118 (1965).
15. M.V. Berry, "Cusped Rainbows and Incoherence Effects in the Rippling-Mirror Model for Particle Scattering from Surfaces," *J. Phys. A: Math. Gen.* **8**, 566-584 (1975).
16. E. Jakeman and J.G. McWhirter, "Fluctuations in Radiation Scattered into the Fresnel Region by a Random-Phase Screen in Uniform Motion," *J. Phys. A: Math. Gen.* **9**, 785-797 (1976).

Appendix A

COHERENCE FUNCTION DEFINITIONS AND PROPAGATION

In this appendix we derive some explicit results for computing the transformed coherence function (or “angular power distribution”)—how it propagates in the absence of surface interaction and how it changes upon encountering a rough interface. Most discussions of the coherence function rely on the parabolic approximation to the Helmholtz equation, thereby choosing a preferred direction of propagation. Since in the bottom-scattering problem there are two “natural” directions, the horizontal propagation direction and the normal to the mean scattering surface, we couch our discussion in terms of the Helmholtz equation to avoid picking a preferred direction. The resulting coherence function can then be computed with respect to arbitrary planes.

In general, the two-point mutual coherence function $\Gamma(r, s)$ is given in terms of the complex pressure field $p(\mathbf{r})$ by

$$\Gamma(\mathbf{r}, \mathbf{s}) = \langle p(\mathbf{r} + \frac{\mathbf{s}}{2}) p^*(\mathbf{r} - \frac{\mathbf{s}}{2}) \rangle. \quad (\text{A1})$$

The angular brackets indicate an average over the ensemble of ocean boundaries, sound-speed profiles, or sources. To begin, we assume that our ensemble is degenerate, having only one member. Since the pressure p obeys the Helmholtz equation

$$\begin{aligned} \nabla^2 p(\mathbf{r} + \frac{\mathbf{s}}{2}) + k_0^2 n^2(\mathbf{r} + \frac{\mathbf{s}}{2}) p(\mathbf{r} + \frac{\mathbf{s}}{2}) &= 0 \\ \nabla^2 p^*(\mathbf{r} - \frac{\mathbf{s}}{2}) + k_0^2 n^2(\mathbf{r} - \frac{\mathbf{s}}{2}) p^*(\mathbf{r} - \frac{\mathbf{s}}{2}) &= 0, \end{aligned} \quad (\text{A2})$$

we find an equation for Γ by multiplying the first of these equations by $p^*(\mathbf{r} - \mathbf{s}/2)$ and the second by $p(\mathbf{r} + \mathbf{s}/2)$ and then subtracting. The result is

$$\begin{aligned} 2 \frac{\partial}{\partial \mathbf{r}} \cdot \frac{\partial}{\partial \mathbf{s}} \Gamma(\mathbf{r}, \mathbf{s}) &= -k_0^2 \left[n^2(\mathbf{r} + \frac{\mathbf{s}}{2}) - n^2(\mathbf{r} - \frac{\mathbf{s}}{2}) \right] \Gamma(\mathbf{r}, \mathbf{s}) \\ &\approx -k_0^2 \mathbf{s} \cdot \nabla n^2(\mathbf{r}) \Gamma(\mathbf{r}, \mathbf{s}). \end{aligned} \quad (\text{A3})$$

The last approximation is called the “locally quadratic” approximation. It is valid when $n^2(\mathbf{r})$ is slowly varying over the domain of the separation variable \mathbf{s} for which Γ is significant. If n^2 is a quadratic function of \mathbf{r} , the locally quadratic approximation is exact.

The solution of Eq. (A3) is found by Fourier transforming with respect to the separation vector \mathbf{s} in three dimensions. (This differs from the more usual procedure of transforming \mathbf{s} over a plane.) We then find that in the locally quadratic approximation the transformed coherence function

$$\hat{\Gamma}(\mathbf{r}, \boldsymbol{\theta}) = \int e^{-ik_0 \boldsymbol{\theta} \cdot \mathbf{s}} \Gamma(\mathbf{r}, \mathbf{s}) d^3\mathbf{s} \quad (\text{A4})$$

satisfies the equation

$$\boldsymbol{\theta} \cdot \frac{\partial}{\partial \mathbf{r}} \hat{\Gamma}(\mathbf{r}, \boldsymbol{\theta}) + \frac{1}{2} \nabla n^2(\mathbf{r}) \frac{\partial}{\partial \boldsymbol{\theta}} \hat{\Gamma}(\mathbf{r}, \boldsymbol{\theta}) = 0. \quad (\text{A5})$$

This first-order linear equation is solved by the method of characteristics. In this case the characteristics turn out to be the rays of geometric acoustics, satisfying the equations

$$\frac{d\mathbf{r}}{d\tau} = \boldsymbol{\theta}, \quad \frac{\partial \boldsymbol{\theta}}{\partial \tau} = \frac{1}{2} \nabla^2 n^2(\mathbf{r}). \quad (\text{A6})$$

The variable τ is related to the arc length of the ray by

$$d\mathbf{s} = n(\mathbf{r}) d\tau. \quad (\text{A7})$$

From the ray equations, Eq. (A6), it follows that ‘‘energy’’ is conserved along the characteristics. That is, if the pairs $(\mathbf{r}, \boldsymbol{\theta})$ and $(\mathbf{r}_0, \boldsymbol{\theta}_0)$ are joined by a ray, then

$$\boldsymbol{\theta}^2 - n^2(\mathbf{r}) = \boldsymbol{\theta}_0^2 - n^2(\mathbf{r}_0). \quad (\text{A8})$$

The vector $\boldsymbol{\theta}$ is tangent to the rays and gives the local direction of energy propagation. The significance of the characteristics for the coherence function is that Eq. (A5) implies that $\hat{\Gamma}$ is constant along characteristics, just as is the ‘‘energy’’ of Eq. (A8).

It is tempting to interpret $\hat{\Gamma}$ as the joint distribution of energy in space and in direction because the marginals of $\hat{\Gamma}$ do indeed give the spatial and angular distribution of energy. However, since $\hat{\Gamma}$ can be negative for some pressure fields, such an interpretation should only be used with great caution. What is more certain is that $\hat{\Gamma}$ contains the acoustic information necessary to determine quadratic functionals of the acoustic field such as outputs of a square-law detector.

Equation (A5) implies that $\hat{\Gamma}$ is constant along the rays of geometric acoustics. Hence

$$\hat{\Gamma}(\mathbf{r}, \boldsymbol{\theta}) = \hat{\Gamma}(\mathbf{r}_0, \boldsymbol{\theta}_0) \quad (\text{A9})$$

where $(\mathbf{r}, \boldsymbol{\theta})$ and $(\mathbf{r}_0, \boldsymbol{\theta}_0)$ are connected by a ray. Note again that $\boldsymbol{\theta}$ is a three-dimensional vector; when the parabolic approximation is used, the vector corresponding to \mathbf{s} is a two-dimensional vector lying in a plane normal to the principal direction of propagation. Here the magnitude, rather than the direction of $\boldsymbol{\theta}$, is restricted by Eq. (A8). To account explicitly for this restriction, we define

$$\gamma(\mathbf{r}, \boldsymbol{\theta}; E) = \delta(\boldsymbol{\theta}^2 - n^2(\mathbf{r}) - E) \hat{\Gamma}(\mathbf{r}, \boldsymbol{\theta}). \quad (\text{A10})$$

Since $\theta^2 - n^2(\mathbf{r})$ is constant along rays as is $\hat{\Gamma}$, it follows that γ is constant along rays. Furthermore, Eq. (A10) implies that $\hat{\Gamma}$ is given in terms of γ by

$$\hat{\Gamma}(\mathbf{r}, \boldsymbol{\theta}) = \int \gamma(\mathbf{r}, \boldsymbol{\theta}; E) dE. \quad (\text{A11})$$

It often happens that information about the pressure field and hence $\hat{\Gamma}$ is restricted to a plane surface. To restrict \mathbf{s} to lie in a particular surface, we can integrate

$$\begin{aligned} \frac{k_0}{2\pi} \int \hat{\Gamma}(\mathbf{r}, \boldsymbol{\theta}) d\boldsymbol{\theta}_\perp &= \int e^{-ik_0\boldsymbol{\theta}_\perp \cdot \mathbf{s}_\perp} \langle p(\mathbf{r} + \frac{\mathbf{s}_\parallel}{2}) p^*(\mathbf{r} - \frac{\mathbf{s}_\parallel}{2}) \rangle d^2\boldsymbol{\theta}_\parallel \\ &= \hat{\Gamma}(\mathbf{r}, \boldsymbol{\theta}_\parallel), \end{aligned} \quad (\text{A12})$$

where \mathbf{s}_\perp is the component of \mathbf{s} perpendicular to the surface in question and \mathbf{s}_\parallel is the component parallel to that surface. Equations (A10) and (A11) can be used to write the restriction of $\hat{\Gamma}$ to a surface as

$$\begin{aligned} \hat{\Gamma}(\mathbf{r}, \boldsymbol{\theta}_\parallel) &= \frac{k_0}{2\pi} \int_{-\infty}^{\infty} \frac{\hat{\Gamma}(\mathbf{r}_0, \boldsymbol{\theta}_{0\parallel}) |_{\theta_{0\perp} = \sqrt{E + n^2(\mathbf{r}_0) - \theta_{0\parallel}^2}}}{2\sqrt{E + n^2(\mathbf{r}) - \theta_\parallel^2}} \\ &= \frac{k_0}{2\pi} \int_{-\infty}^{\infty} \frac{\hat{\Gamma}(\mathbf{r}, \boldsymbol{\theta}_\parallel) |_{\theta_\perp = \sqrt{E + n^2(\mathbf{r}) - \theta_\parallel^2}}}{2\sqrt{E + n^2(\mathbf{r}) - \theta_\parallel^2}}. \end{aligned} \quad (\text{A13})$$

By using

$$E = \theta_{0\perp}^2 + \theta_{0\parallel}^2 - n^2(\mathbf{r}_0) \text{ and } dE = 2\theta_{0\perp} d\theta_{0\perp}, \quad (\text{A14})$$

this equation becomes

$$\hat{\Gamma}(\mathbf{r}, \boldsymbol{\theta}_\parallel) = \frac{k_0}{2\pi} \int \frac{\hat{\Gamma}(\mathbf{r}_0, \boldsymbol{\theta}_{0\parallel}) |_{\theta_{0\perp}} \theta_{0\perp} d\theta_{0\perp}}{\sqrt{\theta_{0\parallel}^2 + \theta_{0\perp}^2 - n^2(\mathbf{r}_0) + n^2(\mathbf{r}) - \theta_\parallel^2}}. \quad (\text{A15})$$

To the extent that $\hat{\Gamma}(\mathbf{r}_0, \boldsymbol{\theta}_0)$ is sharply peaked about $\theta_{0\parallel}^2 + \theta_{0\perp}^2 - n^2(\mathbf{r}_0) = \bar{E}$, we can write Eq. (A15) as

$$\hat{\Gamma}(\mathbf{r}, \boldsymbol{\theta}_\parallel) = \frac{\sqrt{\bar{E} - \theta_{0\parallel}^2 + n^2(\mathbf{r}_0)}}{\sqrt{\bar{E} - \theta_\parallel^2 + n^2(\mathbf{r})}} \hat{\Gamma}(\mathbf{r}_0, \boldsymbol{\theta}_{0\parallel}). \quad (\text{A16})$$

When $\hat{\Gamma}$ is developed from the parabolic approximation, both $\boldsymbol{\theta}$ and $\boldsymbol{\theta}_0$ are associated with normals to vertical planes. In the present development, the plane associated with $\boldsymbol{\theta}$ need not be parallel to that associated with $\boldsymbol{\theta}_0$, and neither is required to be vertical. In practice \bar{E} is taken to be zero.

Scattering of the Coherence Function

When a rough surface is encountered, the angular distribution of energy is suddenly altered and the distribution of scattered energy is a functional of the distribution of incident energy. We therefore make the assumption that the coherence function transform associated with the scattered energy is given by

$$\mathbf{q} \cdot \hat{\mathbf{n}} \hat{\Gamma}_{\text{scat}}(\mathbf{r}_B, \mathbf{q}) = \int \sum (\mathbf{k} - \mathbf{q}) \mathbf{k} \cdot \hat{\mathbf{n}} \Gamma_{\text{inc}}(\mathbf{r}_B, \mathbf{k}) k_0^3 d^3 \mathbf{k}. \quad (\text{A17})$$

The transition kernel Σ is closely related to the differential cross section per unit area. This description of surface scattering is local in the sense that the scattered $\hat{\Gamma}$ at the point Γ_B on the mean scattering plane is determined by the incident $\hat{\Gamma}$ at that same point. In general this is an approximation whose validity is hard to assess. We also note that the definition of $\hat{\Gamma}$ is problematic when the propagation region is bounded, since the Fourier transform that defines $\hat{\Gamma}$ extends over all space while the pressure field is defined only in a limited region of space. One therefore must argue that $\hat{\Gamma}$ is nonzero only over a limited range of the separation variable \mathbf{s} , or that only a limited range of \mathbf{s} affects the transform. Assuming the vectors $\mathbf{r} + \mathbf{s}/2$ lie in the propagation region, the infinite transform of \mathbf{s} presents no real problems. This means that \mathbf{r} must be kept away from the boundaries.

In Eq. (A17), the scattering kernel Σ can be found by considering what happens to a plane wave. We assume that $\hat{\Gamma}$ can be defined in a region near enough to the scattering surface so that in this region the sound speed may be considered to be a constant. We need a region that is large enough so that there is no difficulty in the definition of $\hat{\Gamma}$ but small enough that refraction can be ignored. If such a region exists, we consider the incident plane wave

$$p(\mathbf{r}) = e^{ik_0\mathbf{q}\cdot\mathbf{r}}, \quad (\text{A18})$$

for which the corresponding function $\hat{\Gamma}$ is

$$\begin{aligned} \hat{\Gamma}_{PW}(\mathbf{r}, \boldsymbol{\theta}) &= \left[\frac{2\pi}{k_0} \right]^3 \delta^3(\boldsymbol{\theta} - \mathbf{k}) \\ &= \Gamma_{\text{inc}}(\mathbf{r}, \boldsymbol{\theta}). \end{aligned} \quad (\text{A19})$$

The corresponding scattered field above the highest points of the scattering surface can be written as a superposition of plane waves

$$P_{\text{scat}}(\mathbf{r}) = \int e^{i\mathbf{q}_{\parallel}\cdot\mathbf{r}_{\parallel}} e^{iq_{\perp}r_{\perp}} A(\mathbf{q}_{\parallel}, \mathbf{k}_{\parallel}) d^2q_{\parallel}, \quad (\text{A20})$$

where $q_{\perp} = \sqrt{k_0^2 - q_{\parallel}^2}$, and the subscripts \parallel and \perp refer to components parallel to and perpendicular to the mean scattering surface. If only a finite portion of the scattering surface is rough, the scattering amplitude in the expression

$$P_{\text{scat}}(\mathbf{r}) = \frac{e^{ikr}}{ikr} f(\hat{\mathbf{r}}, \hat{\mathbf{k}}; k_0) \quad (\text{A21})$$

is related to the plane wave amplitudes $A(\mathbf{k}, \mathbf{q})$ by

$$f(\hat{\mathbf{q}}, \hat{\mathbf{k}}; k_0) = 2\pi k_0 q_{\perp} A(\mathbf{q}_{\parallel}, \mathbf{k}_{\parallel}). \quad (\text{A22})$$

The differential cross section σ for such a finite scattering patch is given by

$$\sigma(\mathbf{k} \rightarrow \mathbf{q}) = \frac{|f(\mathbf{q}, \mathbf{k})|^2}{k_0^2} = (2\pi)^2 q_{\perp}^2 |A(\mathbf{q}_{\parallel}, \mathbf{k}_{\parallel})|^2 \quad (\text{A23})$$

from Ref. A1. If ρ such roughness elements per unit area scatter independently and incoherently, then $\rho\sigma$ is the differential cross section per unit area. Correspondingly, if the surface is randomly rough with homogeneous statistics, the fluctuations of the plane-wave scattering amplitudes satisfy

$$\langle \Delta A(\boldsymbol{\phi}_{\parallel} + \frac{\mathbf{q}_{\parallel}}{2}, \mathbf{k}_{\parallel}) \Delta A^*(\boldsymbol{\phi}_{\parallel} - \frac{\mathbf{q}_{\parallel}}{2}, \mathbf{k}_{\parallel}) \rangle = \delta^2(\mathbf{q}_{\parallel}) \Lambda(\boldsymbol{\phi}_{\parallel}, \mathbf{k}_{\parallel}). \quad (\text{A24})$$

The function $\hat{\Gamma}$ that arises from products of the amplitude fluctuations ΔA , $\hat{\Gamma}_{\text{scat}}^{\text{incoh}}$, is given by

$$\hat{\Gamma}_{\text{scat}}^{\text{incoh}}(\mathbf{r}, \boldsymbol{\theta}) = \int e^{-ik_0 \boldsymbol{\theta} \cdot \mathbf{s}} \int e^{i\boldsymbol{\phi}_{\parallel} \cdot \mathbf{s}_{\parallel}} e^{i\boldsymbol{\phi}_{\perp} \cdot \mathbf{s}_{\perp}} \Lambda(\boldsymbol{\phi}_{\parallel}, \mathbf{k}_{\parallel}) d\boldsymbol{\phi}_{\parallel} d_s, \quad (\text{A25})$$

where $\phi_{\perp} = \sqrt{k_0^2 - \phi_{\parallel}^2}$, and where we assume that $|\mathbf{k}_{\parallel}| < k_0$. It follows from Eq. (A25) that $\hat{\Gamma}_{\text{scat}}^{\text{incoh}}$ is given by

$$\hat{\Gamma}_{\text{scat}}^{\text{incoh}}(\mathbf{r}, \boldsymbol{\theta}) = (2\pi)^3 \frac{\delta(1 - |\boldsymbol{\theta}|)}{k_0} \sqrt{1 - \theta_{\parallel}^2} \Lambda(k_0 \boldsymbol{\theta}_{\parallel}, \mathbf{k}_{\parallel}). \quad (\text{A26})$$

On the other hand, if in Eq. (A17) we use

$$\hat{\Gamma}_{\text{inc}}(\mathbf{r}, \boldsymbol{\phi}) = \left(\frac{2\pi}{k_0} \right)^3 \delta^3(\boldsymbol{\phi} - \mathbf{k}),$$

it follows that

$$\boldsymbol{\theta} \cdot \hat{\mathbf{n}} \hat{\Gamma}_{\text{scat}}^{\text{incoh}}(\mathbf{r}, \boldsymbol{\theta}) = (2\pi)^3 (\mathbf{k} \cdot \hat{\mathbf{n}}) \sum^{\text{incoh}}(\mathbf{k} \rightarrow \boldsymbol{\theta}). \quad (\text{A27})$$

Hence we conclude that the scattering kernel for incoherent scattering is given in terms of fluctuations of the scattered plane wave amplitudes by

$$\mathbf{q} \cdot \hat{\mathbf{n}} \sum(\mathbf{k} \rightarrow k_0 \boldsymbol{\theta}) = \theta_{\perp}^2 \frac{\delta(1 - |\boldsymbol{\theta}|)}{k_0} \Lambda(k_0 \boldsymbol{\theta}_{\parallel}, \mathbf{k}_{\parallel}). \quad (\text{A28})$$

By comparing to results for a surface consisting of distinct, incoherent scattering patches, we find that Λ , the strength of the plane-wave amplitude fluctuations, is related to the differential cross section per unit area by

$$\Lambda(p_{\parallel}, q_{\parallel}) = \frac{\rho}{p_{\perp}^2} \sigma(\mathbf{q} \rightarrow \mathbf{p}). \quad (\text{A29})$$

There is also a part of $\hat{\Gamma}$ associated with the average of the plane wave scattering amplitudes, $\langle A(\mathbf{q}, \mathbf{k}) \rangle$. For homogeneous surface statistics, $\langle A(\mathbf{q}, \mathbf{k}) \rangle$ is proportional to a delta function

$$\langle A(\mathbf{q}, \mathbf{k}) \rangle = \delta(\mathbf{k}_{\parallel} - \mathbf{q}_{\parallel}) a(q_{\parallel}). \quad (\text{A30})$$

In the Kirchhoff approximation, for example, $a(\mathbf{q}_{\parallel})$ is given by

$$a(\mathbf{q}_{\parallel}) = e^{-2\sigma^2 q_{\perp}^2}. \quad (\text{A31})$$

The contribution to the scattered function $\hat{\Gamma}$ arising from the coherent scattered amplitudes is

$$\Gamma_{\text{scat}}^{\text{coh}}(\mathbf{r}, \boldsymbol{\theta}) = |a(\theta)|^2 \hat{\Gamma}_{\text{inc}}(\mathbf{r}, \boldsymbol{\theta}_{\text{inc}})$$

or

$$\Gamma_{\text{scat}}^{\text{coh}}(\mathbf{r}, \boldsymbol{\theta}_{\parallel}, \theta_{\perp}) = |a(\theta)|^2 \hat{\Gamma}_{\text{inc}}(\mathbf{r}, \boldsymbol{\theta}_{\parallel}, -\theta_{\perp}). \quad (\text{A32})$$

Energy conservation requires that the incident energy flux equal the total of the scattered energy flux normal to the mean scattering plane. In terms of a and Λ this means

$$|a(q)|^2 + \int_{\mathbf{q}_{\perp}} \frac{k_{\perp}}{\Lambda(\mathbf{k}_{\parallel}, \mathbf{q}_{\parallel})} d^2k_{\parallel} = 1. \quad (\text{A33})$$

In the Kirchhoff approximation, this relationship is only approximately satisfied.

Reference

- A1. D.H. Berman and J.S. Perkins, "The Kirchhoff Approximation and First-Order Perturbation Theory for Rough-Surface Scattering," *J. Acoust. Soc. Am.* **78**, 1045-1051 (1985).

Appendix B

ARRAY SIMULATION AND THE COHERENCE FUNCTION

In this appendix, we show how array response is expressed in terms of the three-dimensional coherence function transform discussed in Appendix A. We confine our discussion to a linear array, but the array may be arbitrarily oriented. The possibility of off-broadside orientation requires use of the three-dimensional coherence function transform.

Let \mathbf{c} be a three-vector that locates the center of a linear array of hydrophones. Let \mathbf{e}_L denote a unit vector pointed along the array. Then, the signal that results from (a) steering the array, (b) shading the array, and (c) summing the steered, shaded fields at each hydrophone is given by

$$A(\theta_s) = \int W(y) p(\mathbf{c} + y\hat{\mathbf{e}}_L) e^{-ik_0 y \sin \theta_s} dy. \quad (\text{B1})$$

The shading function W allows for either discrete or continuous arrays. The pressure p at the point $\mathbf{c} + y\hat{\mathbf{e}}_L$ is denoted as $p(\mathbf{c} + \hat{\mathbf{e}}_L y)$. Often the signal out of an array is squared to form the power. Equation (B1) implies that the power is given by

$$|A(\theta_s)|^2 = \iint W(y_1) W^*(y_2) p(\mathbf{c} + y_1\hat{\mathbf{e}}_L) p^*(\mathbf{c} + y_2\hat{\mathbf{e}}_L) e^{-ik_0(y_1 - y_2) \sin \theta_s} dy_1 dy_2. \quad (\text{B2})$$

This expression contains the product of pressures at two different points and therefore can be expressed in terms of $\hat{\Gamma}$. Changing to mean and difference coordinates, we can write

$$p(\mathbf{c} + y_1\hat{\mathbf{e}}_L) p^*(\mathbf{c} + y_2\hat{\mathbf{e}}_L) = \left[\frac{k_0}{2\pi} \right]^2 \hat{\Gamma} \left(\mathbf{c} + \frac{y_1 + y_2}{2} \hat{\mathbf{e}}_L \right) e^{ik_0(y_1 - y_2) \hat{\boldsymbol{\theta}} \cdot \hat{\mathbf{e}}_L} d^3\theta. \quad (\text{B3})$$

Therefore the array power A^2 is given by

$$|A(\theta_s)|^2 = \int dy ds W\left(y + \frac{s}{2}\right) W^*\left(y - \frac{s}{2}\right) \left[\frac{k_0}{2\pi} \right]^3 \int d^3\theta \hat{\Gamma}(\mathbf{c} + y\hat{\mathbf{e}}_L, \boldsymbol{\theta}) e^{ik_0 s (\hat{\boldsymbol{\theta}} \cdot \hat{\mathbf{e}}_L - \sin \theta_s)}. \quad (\text{B4})$$

A more succinct expression for the power can be obtained by defining an analog of $\hat{\Gamma}$ for the shading functions. Let $a(y, \boldsymbol{\theta}, \theta_s)$ be given by

$$a(y, \boldsymbol{\theta}, \theta_s) = \int W\left(y + \frac{s}{2}\right) W^*\left(y - \frac{s}{2}\right) e^{ik_0 s (\hat{\boldsymbol{\theta}} \cdot \hat{\mathbf{e}}_L - \sin \theta_s)} ds. \quad (\text{B5})$$

Equation (B4) becomes

$$|A(\theta_s)|^2 = \iint a(y, \boldsymbol{\theta}, \theta_s) \hat{\Gamma}(\mathbf{c} + y\hat{\mathbf{e}}_L, \boldsymbol{\theta}) d^3\theta dy. \quad (\text{B6})$$

Note that $a(Y, \boldsymbol{\theta}, \theta_s)$ depends on θ only through $\hat{\mathbf{e}}_L \cdot \hat{\boldsymbol{\theta}} = \sin \psi$. The angle ψ is the arrival angle at the array measured from broadside. It follows that Eq. (B6) simplifies to

$$|A(\theta_s)|^2 = \int \int a(y, \psi, \theta_s) \hat{\Gamma}(\mathbf{c} + y \hat{\mathbf{e}}_L, \theta) d^3 \theta dy. \quad (\text{B7})$$

We assume that by judicious choice of k_0 we can make $\hat{\Gamma}$ sharply spiked about $|\boldsymbol{\theta}| = 1$. By using Eqs. (A10) and (A11), we find

$$|A(\theta_s)|^2 = \int \int a(y, \psi, \theta_s) \frac{\sqrt{E + n^2}}{2} \hat{\Gamma}(\mathbf{c} + y \hat{\mathbf{e}}_L, \psi, \Omega, \theta = \sqrt{E + n^2}) \cos \psi d\psi d\Omega dy dE, \quad (\text{B8})$$

where

$$n^2 = n^2(\mathbf{c} + y \hat{\mathbf{e}}_L).$$

If, in fact, $\hat{\Gamma}$ is proportional to a delta function in E , $\hat{\Gamma} = \hat{\Gamma}_0 \delta(E)$, then

$$|A(\theta_s)|^2 = \int \int \int \frac{1}{2} n^2(\mathbf{c} + y \hat{\mathbf{e}}_L) a(y, \psi, \theta_s) \hat{\Gamma}_0(\mathbf{c} + y \hat{\mathbf{e}}_L, \psi, \Omega) \cos \psi d\psi d\Omega dy \quad (\text{B9})$$

where

$$\hat{\Gamma}_0(\mathbf{r}, \psi, \Omega) = \hat{\Gamma}_0(\mathbf{r}, n(\mathbf{r})) (\sin \psi \hat{\mathbf{e}}_L + \cos \psi \cos \Omega \hat{\mathbf{e}}_H + \cos \psi \sin \Omega \hat{\mathbf{e}}_V). \quad (\text{B10})$$

(The unit vectors $\hat{\mathbf{e}}_H$ and $\hat{\mathbf{e}}_V$ are defined below.)

We model a shaded array of N discrete hydrophones located at positions along the array, y_i , by

$$W(y) = \sum_i W_i \delta(y - y_i). \quad (\text{B11})$$

The shading function applied to each hydrophone is denoted w_i . The function $a(y, \psi, \theta_s)$ that summarizes intrinsic array properties is now given by

$$a(y, \psi, \theta_s) = \sum_{i,j} \delta(y - \frac{y_i + y_j}{2}) w_i w_j^* e^{-ik_0(y_i - y_j)(\sin \theta_s - \sin \psi)}. \quad (\text{B12})$$

Note that a is nonzero not only at hydrophone positions but also between hydrophone positions at $(y_i + y_j)/2$. By using this expression for a , the array power can be written

$$|A(\theta_s)|^2 = \sum_{i,j} \int \int \frac{1}{2} n^2(\mathbf{c} + \frac{y_i + y_j}{2} \hat{\mathbf{e}}_L) a(y, \psi, \theta_s) \hat{\Gamma}_0(\mathbf{c} + \frac{y_i + y_j}{2} \hat{\mathbf{e}}_L, \psi, \Omega) \cos \psi d\psi d\Omega. \quad (\text{B13})$$

Equation (B13) is the central result of this appendix.

The function a summarizes the intrinsic array properties. We now comment on the description of the array geometry. We have denoted a unit vector pointing along the array by $\hat{\mathbf{e}}_L$. Let $\hat{\mathbf{z}}$ be the unit vector pointing downward. We define a unit horizontal vector perpendicular to the array by

$$\hat{\mathbf{e}}_H = \frac{\hat{\mathbf{e}}_L \times \hat{\mathbf{z}}}{|\hat{\mathbf{e}}_L \times \hat{\mathbf{z}}|}. \quad (\text{B14})$$

If there is no array yaw, $\hat{\mathbf{e}}_H$ points generally in the direction from the receiver back to the source. A third orthogonal array fixed coordinate is defined by $\hat{\mathbf{e}}_H \times \hat{\mathbf{e}}_L = \hat{\mathbf{e}}_V$. The angles ψ and Ω are chosen so that an arbitrary direction of arriving energy $\hat{\boldsymbol{\theta}}$ can be written

$$\hat{\boldsymbol{\theta}} = \sin \psi \hat{\mathbf{e}}_L + \cos \psi \cos \Omega \hat{\mathbf{e}}_H + \cos \psi \sin \Omega \hat{\mathbf{e}}_V. \quad (\text{B15})$$

If the array is yawed by an amount α and then tilted by an amount β (order is important for rotations!), then $\hat{\mathbf{e}}_L$ is given by

$$\hat{\mathbf{e}}_L = -\sin \alpha \cos \beta \hat{\mathbf{x}} - \cos \alpha \cos \beta \hat{\mathbf{y}} + \sin \beta \hat{\mathbf{z}}. \quad (\text{B16})$$

In similar fashion, the array-fixed unit vectors $\hat{\mathbf{e}}_H$ and $\hat{\mathbf{e}}_V$ can be expressed in terms of α , β , and the space-fixed unit vectors $\hat{\mathbf{x}}$, $\hat{\mathbf{y}}$, $\hat{\mathbf{z}}$.

If energy arrives along the unit vector

$$\hat{\boldsymbol{\theta}} = \cos \theta \cos \phi \hat{\mathbf{x}} - \sin \theta \cos \phi \hat{\mathbf{y}} + \sin \phi \hat{\mathbf{z}}, \quad (\text{B17})$$

then

$$\begin{aligned} \hat{\mathbf{e}}_L \cdot \hat{\boldsymbol{\theta}} &= \cos \beta \cos \phi \sin(\theta - \alpha) + \sin \beta \sin \phi \\ &= \sin \theta'. \end{aligned} \quad (\text{B18})$$

Thus if $\alpha = 0$, $\sin \psi = \hat{\mathbf{e}}_L \cdot \hat{\boldsymbol{\theta}} = \sin \theta'$. This is Eq. (11) of the text. Similar considerations are required to map directions ψ and Ω specified relative to array-fixed axes into angles relative to space-fixed axes. Finally note that the angle defined in Eq. (B15) is the cone angle appearing in Eq. (B13) and in Fig. 2.

Appendix C

TRACING THE CHARACTERISTIC PATHS

The tracing algorithm used in ORBS computes closed-form solutions for layer-to-layer path increments in a range-independent stratified sound-speed structure, so that the paths may be computed efficiently for a general multilayer deep-ocean profile. The profile is entered as a set of depth-sound speed pairs $\{z_i, c_i\}$, and an interpolating function of the form

$$c(z) = c_i [1 - 2g_i(z - z_i)]^{-1/2}, \quad z_i \leq z \leq z_{i+1} \quad (C1)$$

is used; g_i is a fitting parameter for the i th layer. One way of expressing the solution for the path for this interpolating function [C1] is

$$\tan \phi = \tan \phi_i - rg_i (c_m/c_i)^2, \quad (C2)$$

where ϕ is the angle measured down from the horizontal, r is the range in the i th layer (the path enters the layer with angle ϕ_i), and the parameter c_m is defined by Snell's Law:

$$c = c_m \cos \phi. \quad (C3)$$

In addition to the layer-by-layer trace of path increments, we need an efficient way of tracing a path to its intersection with the bottom. In ORBS, this is done by assuming that the paths contact the bathymetry only in deep water ($z \geq 3000$ m), where the depth gradient of the sound speed is approximately constant and a simplified tracing algorithm can be used. The bottom layer of the profile is fitted to the linear interpolating function

$$c(z) = C + Gz. \quad (C4)$$

Then, the path solution can be written

$$\sin \phi = \sin \phi_i - rG/c_m, \quad (C5)$$

where ϕ , ϕ_i and c_m are as defined above, and r is the range in the bottom layer. Now suppose the mean bottom plane intersects the vertical plane of the path in a line whose equation is

$$z = z_0 + hr. \quad (C6)$$

To find the point where the path intersects the bottom plane, define c_b as the sound speed at the bottom intersection and combine the last three equations (and Snell's Law) to obtain a quadratic in c_b :

$$(l + h^2)c_b^2 - 2Bc_b + B^2 - (hc_m)^2 = 0, \quad (C7)$$

where $B = C + Gz_0 + hc_m \sin \phi_i$. This equation can be solved by the quadratic formula. (If no solution exists, the path misses the bottom and is not a contributor to the scattered or reflected energy.) The range and depth of the bottom hit are now linear functions of c_b .

Reference

- C1. M.A. Pedersen and D.F. Gordon, "Normal-Mode Theory Applied to Short-Range Propagation in an Underwater Acoustic Surface Duct," *J. Acoust. Soc. Am.* **37**, 105-118 (1965).

Appendix D
COMPUTING THE SCATTERING CROSS SECTION

The scattering cross section governs the fraction of energy impinging upon the bottom that is scattered in each direction. It is a function of the bathymetric spectrum and the direction of the incoming energy. The model incorporated in ORBS is based on a combination of small perturbation theory and the Kirchhoff approximation [D1]. This model reduces to perturbation theory for small surface heights and to conventional Kirchhoff theory for gently undulating surfaces with large surface heights. Thus, the region of validity of the model is at least as great as the union of the regions of validity of its limiting forms.

Let \mathbf{q} be the wave vector incident upon the bottom and let \mathbf{k} be the wave vector in a scattered direction. According to Kirchhoff theory, the proportion of the incident energy reflected coherently (in the specular direction) is given by

$$R_{\text{refl}} = e^{-4q_z^2\sigma^2}, \quad (\text{D1})$$

where q_z is the component of \mathbf{q} normal to the mean surface, and σ is the rms residual bottom height. The remainder of the incident energy is scattered in the nonspecular directions. The cross section per unit area for incoherent scattering from the incident direction \mathbf{q} to the scattered direction \mathbf{k} may be written [D1]:

$$\sigma(\mathbf{q} \rightarrow \mathbf{k}) = \frac{1}{16\pi^2 q_z} \{b_1^2 I_{1,1} + 2R b_1 b_{-1} I_{1,-1} + b_{-1}^2 I_{-1,-1}\}, \quad (\text{D2})$$

where R is an elastic coefficient between -1 (perfectly soft bottom) and $+1$ (perfectly hard bottom) and

$$I_{mn} = \int \exp [i(\mathbf{q} - \mathbf{k}) \cdot \mathbf{r}] \{ \exp [\lambda_m \lambda_n \sigma^2 W(r)] - 1 \} / (\lambda_m \lambda_n) d^2 r, \quad (\text{D3a})$$

$$\lambda_m = q + mk, \quad m = \pm 1, \quad (\text{D3b})$$

and

$$b_m = [(q_z + mk_z)^2 + |\mathbf{q}_{\parallel} - \mathbf{k}_{\parallel}|^2] \exp (-\lambda_m^2 \sigma^2 / 2). \quad (\text{D3c})$$

In the Eqs. (D3), the subscript z designates the component of a vector normal to the mean surface, and the subscript \parallel designates the components parallel to the surface. The function $W(\mathbf{r})$ in Eq. (D3a) is the normalized correlation function of surface-height fluctuations,

$$W(\mathbf{r}) = \langle h(\mathbf{r})h(0) \rangle / \langle h^2(0) \rangle, \quad (\text{D4})$$

where $h(\mathbf{r})$ is the height of the scattering surface above the point specified by the two-dimensional vector \mathbf{r} in some reference plane. The two-dimensional surface height spectrum is defined by a two-dimensional Fourier transform of $W(\mathbf{r})$:

$$S(\mathbf{k}) = \sigma^2 \iint \exp(i\mathbf{k} \cdot \mathbf{r}) W(\mathbf{r}) d^2r, \quad (\text{D5})$$

where the rms surface roughness $\langle h^2(0) \rangle$ is denoted by σ^2 . By inversion of the transform of Eq. (D5), $W(\mathbf{r})$ satisfies

$$W(\mathbf{r}) = (2\pi\sigma)^{-2} \exp(-i\mathbf{k} \cdot \mathbf{r}) S(\mathbf{k}) d^2k. \quad (\text{D6})$$

In the examples to follow, consider the isotropic bathymetric correlation function

$$W(r) = (r/L_c) K_1(r/L_c), \quad (\text{D7})$$

where K_1 is the first-order modified Bessel function of the second kind, as a function of the scalar separation $r = |\mathbf{r}|$. This choice of $W(r)$ corresponds to a k^{-4} dependence in the high-wave-number region of the spectrum; specifically, the spectrum obtained by transforming Eq. (D7) is

$$S(k) = 4\pi(\sigma L_c)^2 [1 + (kL)^2]^{-2}, \quad (\text{D8})$$

where $k = |\mathbf{k}|$ and L_c is the correlation length of the bottom height variations about the reference plane. (Other choices for $W(r)$ may be considered, such as a Gaussian, which makes $S(k)$ a Gaussian also.)

Figure D1 shows the results of cross-section calculations with the correlation function and spectrum of Eqs. (D7) and (D8), with $L_c = 1600$ m, $\sigma = 30$ m, and for a 100 Hz source impinging at a grazing angle of 20° to the mean bottom. For such a large roughness, we would not expect perturbation theory to be accurate but would expect Kirchhoff theory to be valid. The cross section is plotted in Fig. D1, where the modified Kirchhoff result is plotted on the top as a function of outgoing vertical and azimuthal angles, and the corresponding perturbation and standard Kirchhoff results are below. The plot also shows the position and value of the maximum of each of the three formulations. As expected, the modified Kirchhoff calculation is accurate in this region (as shown by comparison with the standard Kirchhoff result), while perturbation theory is in error by several orders of magnitude. Further examples are contained in Ref. D2.

As stated in Section 2, hundreds of thousands of evaluations of the cross section are needed in a typical ORBS calculation. The most time-consuming part of the calculation is the numerical computation of the integral in Eq. (D3a), which is needed for Eq. (D2). We have simplified the calculation by a technique that falls into the class of approximations called exponential substitution [D3,D4]. The integral to be evaluated is of the form

$$I(\mathbf{Q}) = \iint \exp(i\mathbf{Q} \cdot \mathbf{s}) \{ \exp[HW(\mathbf{s})] - 1 \} d^2s. \quad (\text{D9})$$

We assume that we can approximate this integral by

$$J(\mathbf{Q}) = \iint \exp(i\mathbf{Q} \cdot \mathbf{s}) \Lambda W(\mathbf{s}/s_0) d^2s, \quad (\text{D10})$$

where Λ and s_0 are parameters to be chosen. With a change of variables we obtain

$$J(\mathbf{Q}) = s_0^2 \Lambda \iint \exp(is\mathbf{Q} \cdot \mathbf{x}) W(\mathbf{x}) d^2x. \quad (\text{D11})$$

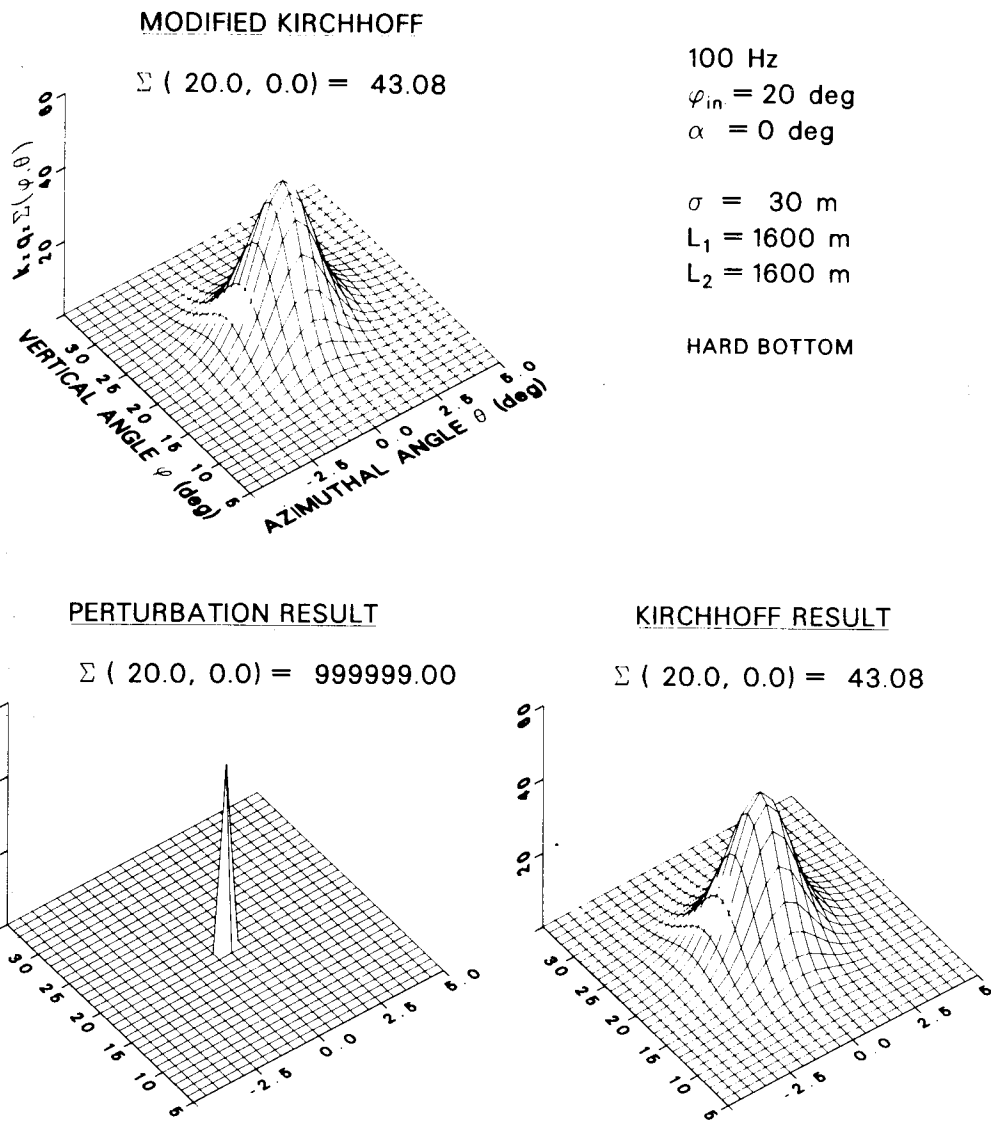


Fig. D1 — Scattering cross section as a function of vertical and azimuthal angles obtained by using the exact formulation

The integral in Eq. (D11) is the two-dimensional Fourier transform of the bathymetric correlation function, which by definition gives the bottom-height spectrum S (Eq. (D5)), that is,

$$J(\mathbf{Q}) = s_0^2 \Lambda S(\mathbf{Q}s_0)/\sigma^2 \quad (\text{D12})$$

We now choose Λ so that the integrands of I and J are equal for $s = 0$, obtaining

$$\Lambda = \exp(H) - 1. \quad (\text{D13})$$

There are many ways to choose s_0 . It is convenient and accurate to require that

$$J|_{\mathcal{Q}=0} = I|_{\mathcal{Q}=0}. \quad (\text{D14})$$

This means that the approximation is exact in the specular direction. The result is

$$s_0 = \left\{ \frac{\sigma^2 \iint \exp [HW(s) - 1] d^2s}{S(0)(e^H - 1)} \right\}. \quad (\text{D15})$$

This defines s_0 as a function of H that in general is very smooth and readily tabulated. Its evaluation is then simply a matter of table look-ups and interpolation. Because as $S(k)$ is often given in a simple closed form (for example, if W is Gaussian or as in Eq. (D7)), the evaluation of the cross section, Eq. (D2), is greatly reduced in complexity by exponential substitution.

Figure D2 shows the result of using the approximation for the same case as Fig. D1. The differences in the modified Kirchhoff result between Figs. D1 and D2 are minimal. The peak values (for $\mathbf{Q} = \mathbf{q} - \mathbf{k} = 0$) are virtually identical, but of course this is one of the conditions set by Eq. (D13). The difference in total scattered energy corresponding to the two functions, computed by numerical integration, is $< 7\%$. On a VAX-11/780 computer, it took 90 min of CPU time to calculate the results in Fig. D1, while Fig. D2 took ~ 90 s, with a significant percentage taken up in the plotting. Thus, using this approximation reduces computational time by almost two orders of magnitude.

The bathymetric statistics are easily generalized to model an anisotropic bottom. An example of an anisotropic bottom spectrum with different correlation lengths in the x - and y -directions is

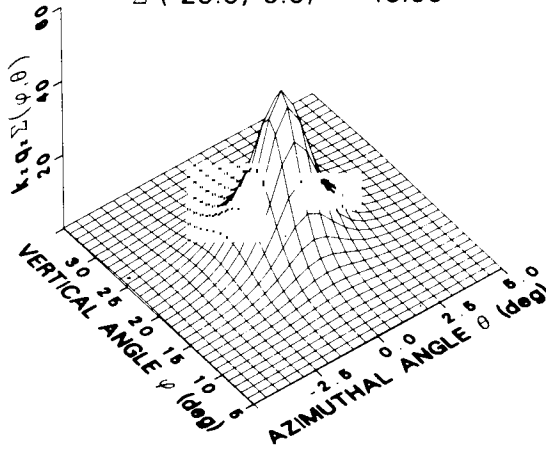
$$S(\mathbf{k}) = 4\pi\sigma^2 L_{xy}^2 [1 + k^2 L_{xy}^2]^{-2}, \quad (\text{D16})$$

where the vectors $\mathbf{L} = (L_x, L_y)$ and $\mathbf{k} = (k_x, k_y)$ and $L_{xy}^2 = L_x L_y$. This spectrum is a generalization of the spectrum of Eq. (D7). It has the same k^{-4} dependence in the high-wave-number tail when evaluated along either principal axis in k -space. By use of the coordinate transformation $\mathbf{k}' = (k_x \sqrt{L_x/L_y}, k_y \sqrt{L_y/L_x})$, the transform integral for the correlation function (Eq. (D6)) can put into the same form as the isotropic case, and the correlation function $W(\mathbf{r})$ is equal to

$$W(\mathbf{r}') = (r'/L_{xy}) K_1(r'/L_{xy}), \quad (\text{D17})$$

MODIFIED KIRCHHOFF

$\Sigma (20.0, 0.0) = 43.05$



100 Hz

$\varphi_{in} = 20 \text{ deg}$

$\alpha = 0 \text{ deg}$

$\sigma = 30 \text{ m}$

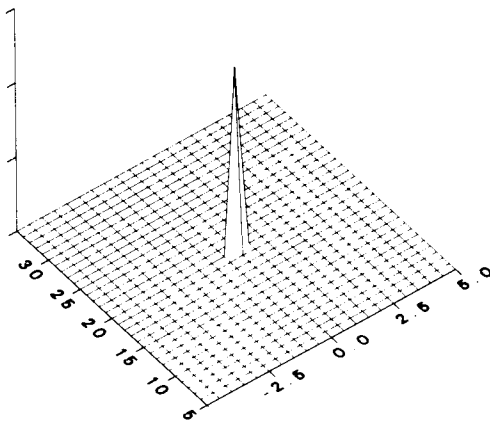
$L_1 = 1600 \text{ m}$

$L_2 = 1600 \text{ m}$

HARD BOTTOM

PERTURBATION RESULT

$\Sigma (20.0, 0.0) = 999999.00$



KIRCHHOFF RESULT

$\Sigma (20.0, 0.0) = 43.05$

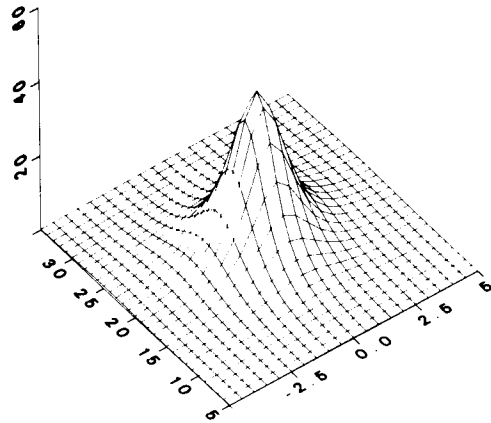


Fig. D2 — Scattering cross section as a function of vertical and azimuthal angles obtained by using the exponential substitution approximation

where the vector $\mathbf{r}' = (x \sqrt{L_y/L_x}, y \sqrt{L_x/L_y})$, and $r' = |\mathbf{r}'|$. Then the Kirchhoff integral assumes the same form as in the isotropic case, and the same method of exponential substitution outlined above can be used to approximate it. The result is that $J(\mathbf{Q})$ is equal to

$$J(\mathbf{Q}') = \Lambda s_0^2 S(s_0 \mathbf{Q}') / \sigma^2, \quad (\text{D18})$$

where the vector $\mathbf{Q}' = (Q_x \sqrt{L_x/L_y}, Q_y \sqrt{L_y/L_x})$. Anisotropic bottom statistics are thus introduced by specifying two correlation lengths in the principal directions and using them to define a scale change in the coordinate system in k -space. This type of anisotropic spectrum could be used to represent, for example, a sloping bottom with furrows running along the direction of the slope. This would be the direction with larger correlation length.

References

- D1. D.H. Berman and J.S. Perkins, "The Kirchhoff Approximation and First-Order Perturbation Theory for Rough-Surface Scattering," *J. Acoust. Soc. AM.* **78**, 1045-1051 (1985).
- D2. Stanley M. Flatté, ed., *Sound Transmission through a Fluctuating Ocean* (Cambridge University Press, 1979).
- D3. M.V. Berry, "Cusped Rainbows and Incoherence Effects in the Rippling-Mirror Model for Particle Scattering from Surfaces," *J. Phys. A: Math. Gen.* **8**, 566-584 (1975).
- D4. E. Jakeman and J.G. McWhirter, "Fluctuations in Radiation Scattered into the Fresnel Region by a Random-Phase Screen in Uniform Motion," *J. Phys. A: Math. Gen.* **9**, 785-797 (1976).

Appendix E

PROGRAM DATA INPUTS

This appendix consists of an outline of the input data for ORBS and a sample data file.

There are two ways of specifying a field of coherence-function values to start up the program:

- The program can read from a binary file of values of the coherence function transform, computed from a PE computation, for a PE computation for a succession of source-cylinder ranges. This allows the source-receiver range to be varied for a given computed sound field.

- A simulated field can be used. The energy at the source cylinder is distributed in a two-dimensional Gaussian about a mean depth and a mean vertical direction. In this case the random-access file and FORTRAN unit 4 are not needed. The flag for choosing the startup method is on record 4.

Read in the data in the following series of card images (note that it was considered convenient to use the format (10F8) for all data):

Record 1: Any alphanumeric title in columns 1-72

Record 2: RPKM,RCKM,ZC,ALPHAD,BETAD,XL,XN,XMODE

RPKM	—	Source cylinder range (km)
RCKM	—	Range (km) of center of array (point C)
ZC	—	Depth (m) of point C
ALPHAD	—	Array yaw (rotation about vertical) (deg). Zero yaw means the array is broadside to the source. Positive yaw is counterclockwise as seen from above.
BETAD	—	Array tilt (deg) in vertical plane about point C. Positive tilt is clockwise as seen from the source.
XL	—	Length of array (m)
XN	—	Number of phones in array
XMODE	—	A flag 0. to 7.: set 4-bit to omit direct paths set 2-bit to omit reflected paths set 1-bit to omit scattered paths (But enter with decimal point)

Record 3: SIGMAS,CLX,CLY,ZBC,ZMAX,SLOPED,YAWD,SPOW,GAMMAD

- SIGMAS — rms roughness (m) of the bottom; i.e., the standard deviation of residual bottom heights about mean bottom plane
- CLX — Correlation length (m) of residual bottom height distribution, measured in slope direction in mean bottom plane
- CLY — Correlation length (m) of bottom height distribution, measured in cross-slope direction in mean bottom plane. Note that these measurement directions can be rotated by specifying a nonzero skew angle. For an isotropic bottom, enter CLY equal to CLX (see GAMMAD).
- ZBC — Depth of mean bottom plane (m) directly under the array center
- ZMAX — Maximum water depth (m)
- SLOPED — Slope (deg) of mean bottom plane. A positive slope is downward from receiver toward source.
- YAWD — Yaw (rotation about vertical) (deg) of bottom. Zero yaw means isobaths in the mean bottom plane are broadside to the source. Positive yaw is counterclockwise as seen from above.
- SPOW — Inverse power-law exponent for bottom roughness spectrum. ORBS models a power spectral density for residual bottom heights asymptotic to k^{**} (-SPOW), where k is the spatial wave number. Values of 4, 5, and 6 may be used for power-law spectra; a value of 0 will cause a Gaussian spectrum to be used. (These are the only values for which tables for the exponential substitution algorithm have been provided.)
- GAMMAD — Roughness ellipse skew angle (deg) (CCW from above). If $CLX = CLY$, the value of GAMMAD is irrelevant (enter zero in this case).

Record 4: FHZ, GAMO, ZS, SIGZS, SBEAMD, SIGSBD, XNSVP

- FHZ — Acoustic frequency (Hz).
- GAMO — Peak value for simulated coherence function at the source cylinder, as described above. (Recommended value: 1.0 to use simulated source; put GAMO = 0. to use the PE-generated startup file.)
- ZS — Depth (m) of peak coherence function value for simulated beamed source
- SIGZS — Standard deviation in depth (m) of Gaussian distribution for simulated beamed source

- SBEAMD — Angle (deg) of peak coherence function value for simulated beamed source. A0 is positive for a beam directed downward from the source.
- SIGSBD — Standard deviation in angle (deg) of Gaussian distribution for simulated beamed source

(The values of ZS, SIGZS, SBEAMD, and SIGSBD are irrelevant if GAMO = 0.)

- XNSVP — Number of depth-sound speed pairs in profile to follow

Record 5: PSI1D,DPSI,PSI2D, OMEGA1D,DOMEGAD,OMEGA2D, DGRZD

- PSI1D — Minimum beam angle (deg) for calculation
- DPSID — Beam angle increment (deg)
- PSI2D — Maximum beam angle (deg) for calculation
- OMEGA1D — Minimum depression angle in beam cone (deg)
- DOMEGAD — Depression angle increment (deg)
- OMEGA2D — Maximum depression angle in beam cone (deg)
- DGRZD — Angle increment (deg) in incident fan of paths from scattering point to source cylinder

Record 6: (Z(L), C(L), L = 1, NSVP)

- Z — Array of depths (m) for sound speed profile
- C — Array of corresponding sound speeds (m/s)

